P AND S WAVE VELOCITY DETERMINATION

M.E. Willis and M. N. Toksöz

Earth Resources Laboratory
Department of Earth and Planetary Sciences
Massachusetts Institute of Technology
Cambridge, MA 02139

ABSTRACT

There are three general methods that can be used to determine formation velocities from full waveform logs. The first approach is to make use of the data from the entire waveform. This type of velocity analysis is performed either in the frequency domain (i.e. f-k analysis or the two station method) or in the time domain (i.e. velocity spectral analysis). The second approach is to identify the P wave pulses on individual traces and to determine delay times between traces. In conventional acoustic logging this technique has been used successfully to determine the compressional wave velocities. The third approach is to use the phase velocity of the guided waves (Pseudo-Rayleigh) to determine the shear velocity. Each of these approaches have certain advantages and limitations depending on the tool characteristics (number of records, frequency response), formation properties (high or low shear velocity), and computation times required. The effect of these parameters upon each method of velocity determination is presented.

INTRODUCTION

One application of full waveform acoustic logs is the determination of the P and S wave velocities in the borehole. In situ velocity data from full waveform acoustic logs can be used in conjunction with other well logs to calculate Poisson's ratio and to estimate formation porosity and permeability. This paper examines three different approaches to velocity determinations, compares their performance using synthetic test data and applies the selected P and S wave methods to data from three different wells.

Synthetic data was used to test the accuracy of the methods discussed in this paper. A suite of synthetic waveforms for several formations were generated using the method developed by Cheng and Toksöz (1981) and Cheng et al. (1982) for synthetic acoustic waveforms in the borehole. The method generates seismograms for a fluid-filled borehole in a homogeneous formation from a point source in the center of the borehole. While this calculation does not include a tool in the hole, they show that an effective tool radius can be subtracted from the borehole radius to match actual waveforms. The synthetic data was generated for an 8 and 10 ft (2.44 and 3.05 m) source receiver offset. Table 1 gives the other model parameters.

The synthetic data are not noise-free due to the effects of spectral and temporal aliasing, numerical approximation, and round-off error. Their signal to noise levels, however, have been estimated. The ratio of the peak P wave signal to RMS background noise before its arrival gives an average signal to noise level of 18db.

FULL WAVEFORM METHODS

If a logging tool has 10 or more receivers, P and S wave velocities can be determined by frequency-wavenumber analysis of the recorded waveforms. This method separates and identifies the various modes, namely the Stoneley, pseudo-Rayleigh, and body waves, and determines their dispersion and velocity characteristics. This scheme necessitates data from many closely-spaced receivers. If, however, data are available at a limited number of spacings (three in our case), an f-k analysis looses resolution and may become spatially aliased. In such a case the phase velocity method commonly used in earthquake seismology may be applicable (Brune, et. al. 1960).

Phase Velocity Techniques

Figure 1 is a schematic of the borehole geometry showing the travel paths of the headwaves through the system. The recorded waveform at receiver numbers 1 and 2 are denoted as r_1 and r_2, respectively. The waveforms recorded can be decomposed into smaller subsystems which comprise the different legs of the travel path. This gives

$$r_1 = S_1 * L_1 * L_2 * L_3 * R_1 \tag{1}$$

$$r_2 = S_1' * L_1 * L_2 * D * L_4 * R_2$$

where S_1= source waveform for the first firing
S_1'= source waveform for the second firing
R_1= receiver number one response
R_2= receiver number two response
$*$= the convolutional operator

The following assumptions are made:

$$S_1 = S_1'$$

$$L_3 = L_4 \tag{2}$$

$$R_1 = R_2$$

which yields:

$$r_1 = S_1 * L_1 * L_2 * L_3 * R_1$$

$$r_2 = S_1 * L_1 * L_2 * D * L_3 * R_1 \tag{3}$$

$$r_2 = r_1 * D$$

An estimate of D, the impulse response of the formation between the receivers, is calculated by employing Wiener deconvolution. Conceptually this amounts to division in the frequency domain:

$$D(f)=\frac{r_2(f)}{r_1(f)} \tag{4}$$

For headwaves, D should be a unit delay operator, corresponding to the formation velocity, multiplied by the geometric spreading factor $\frac{Z_1}{Z_2}$ where Z_i is the source/receiver offset for the i^{th} receiver (Roever *et al.*, 1974, Winbow, 1980). D will deviate from this due to dispersion or contamination by other wavetypes. For the guided waves, D should exhibit the dispersion associated with the borehole waveguide.

Once the impulse response function has been determined the phase velocity can be calculated. From equation 4 the phase of D, φ_D, is

$$\varphi_D=\varphi_{r_2}-\varphi_{r_1}$$

which is the phase delay of the system, where φ_{r_1} and φ_{r_2} are the Fourier phases of receivers r_1 and r_2.

The phase velocity can then be calculated by

(1) Determining D, as described above by Wiener deconvolution from $r_2=r_1*D$.

(2) Unwrapping the phase spectrum of the fast Fourier transform of D by adaptive integration (Tribolet, 1977).

(3) Determining the phase velocity from

$$c(f)=\frac{f\,\Delta z}{\frac{\varphi_D}{2\pi}+n} \tag{5}$$

where Δz = receiver spacing
φ_D = unwrapped phase spectrum of D
n = arbitrary constant
f = frequency
c = phase velocity

If only the phase of the impulse response function is of interest, it may be determined directly from the Fourier phase differences of r_1 and r_2. In this case the phase velocity may be determined by:

(1) Calculating the fast Fourier transform of r_1 and r_2.

(2) Unwrapping phase spectra of r_1 and r_2 by adaptive integration.

(3) Determining phase velocity from

$$c(f)=\frac{2\pi f\,\Delta z}{\varphi_{r_2}-\varphi_{r_1}+n2\pi} \tag{6}$$

Taylor and Toksöz (1982) show that these two methods give nearly identical phase velocities on noise free and noise contaminated synthetic Love wave records. Selection of the method used to calculate the phase velocity should therefore be based on the relative computation times. Wiener deconvolution requires time proportional to N^2 multiplications (Levinson, 1947), where N is the number of points in the time series. A fast Fourier transform requires time proportional to $N\log_2 N$ multiplications, and adaptive integration proportional to $N\log_2 N+2N^2+21N$ multiplications, $N+1$ double precision logarithms, $2N+1$ double precision arctangents, and $2N^2$ trigonometric function calls. The relative computation times are:
Wiener deconvolution:

$$(3N^2+2N\log_2 N+21N)\alpha+(N+1)\beta+(2N+1)\gamma+(2N^2)\delta$$

Fourier phase differences:

$$(4N^2+4N\log_2 N+42N)\alpha+2(N+1)\beta+(4N+2)\gamma+(4N^2)\delta$$

where α, β, γ, δ, are the computation times for multiplication, double precision logarithm, double precision arctangent, and trigonometric function calls, respectively. Johnston pointed out that more stability is gained in adaptive integration when the number of points in the time series is increased by 2 (Johnston, personal communication, 1980). This is accomplished by adding zeros to the end of the time series and the results halve the frequency interval in the transformed domain. The number of points should therefore be increased for both methods, and the above computer times can just be multiplied by a factor of two.

In summary, it appears that the reduction in the number of adaptive integrations more than compensates for the increase in computer time of the Wiener filter. It is therefore worth while to compute D and realize a computation time savings of $(N^2+21N)\alpha+(N+1)\beta+(2N+1)\gamma+(2N^2)\delta$.

The two station velocity technique can best be exemplified using the test synthetic waveforms. Figure 2 shows the R1 and R2 receiver waveforms. The first nine cycles of the pseudo-Rayleigh wave on each record has been selected for this analysis. The complete guided-wave train cannot be used because it includes the Stoneley wave. A 70 μsecond cosine taper was applied to the edges of the windows. The corresponding windowed waveforms are shown in Figures 3a and 4a. These windows correspond to the portion of the pseudo-Rayleigh wave which arrives after the S wave and before the Stoneley wave. Figures 3 and 4 also show the amplitude and phase spectra of the selected portions of R1 and R2 waveforms.

Figure 5 shows the Wiener filter computed for the windowed waveforms along with its amplitude and phase spectra. Comparison of the spectra of R1 and R2 with that of the Wiener filter reveals a considerable amount of energy outside of the bandwidth of interest in the Wiener filter. Care must be taken to use only the portion of the filter spectrum which contains valid information.

Most of the energy for R1 and R2 is concentrated between about 13 kHz to 15 kHz. Figure 6 shows the phase velocity determined from the Wiener filter in this frequency range using two different values of n: $n = -1$ and $n = 0$. The latter gives velocities less than 7.5 kft/sec. A value for n of -2 gives phase velocities greater than 15 kft/sec (4.5 km/s) which is clearly unreasonable. The value of n therefore is fairly well constrained. The S wave velocity is calculated at approximately 10.45 kft/sec at 12.8 kHz which is in excellent agreement with the model velocity of 10.5 kft/sec.

For completeness, Figure 7 shows a comparison of the phase velocity using equation 6 and that using the Wiener filter from Figure 6. The dashed line shows the velocity using the Fourier phase spectra from the two waveforms utilizing two phase unwrappings. The value of n was -1. as before. Clearly these velocities are almost identical to those using the Wiener filter phase.

Velocity Spectral Analysis

Given data from a number of receivers a velocity spectral analysis, which is used routinely in reflection seismology, can be used to process full waveform acoustic data (Taner and Koehler, 1969). The time-distance function is, however, changed from a hyperbolic reflection moveout to a linear refraction moveout. For a small time window on the first record, the method searches across the other records for coherent energy by sweeping through a range of velocities. The method calculates the semblance at each velocity scanned and plots it as a function of velocity next to the time corresponding to the beginning of this window on the first record. This time window is then moved by increments down the first record and the coherency measurements are plotted for each window.

To illustrate this technique, five synthetic acoustic waveforms were generated for source/receiver separations of 8, 8.5, 9., 9.5, and 10 feet. The formation modeled has a high velocity. The other model parameters are the same as Model a) in Table 1. A velocity analysis of these five records is shown in Figure 8a. The 8 foot record is plotted on the right side of the figure. Note how the P and S velocities are prominent at 19.5 and 10.5 kft/sec.

Figure 8b shows that slower coherent multiple cycle skipping events appear when the number of records analyzed is reduced to two. When the analysis was performed on the 8 and 10 foot records. P and S velocities are still visible, but the S may be confused with the first multiple cycle skip of the P wave at about 12.0 kft/sec.

An example of this analysis on the field data is shown is Figure 8c. There is a clear change from P wave energy at approximately 16,900 ft/sec to the S wave at approximately 10,200 ft/sec. This analysis used 4 records at 3 different source/receiver distances. The first cycle skip of the P wave again confuses the onset of the shear energy. The obvious solution is, of course, that more receivers are needed. The multiple receiver distance analysis simplifies the identification of the S wave velocity by reducing the spatial aliasing.

P WAVE VELOCITY DETERMINATIONS

Conventional P wave sonic logging employs an analog threshold detection device in the recording truck to pick the onset of the P wave at each receiver. Whenever the amplitude of a receiver output exceeds the detection threshold it is assumed that a "P wave" has been identified. In full waveform acoustic logs, the limited dynamic range generally prevents arbitrarily increasing the P-wave amplitude. As a result, the arrival time chosen at each receiver may not correspond to the same portion of the P waveform. This problem typically introduces as much as 10 μsec/ft error in the recorded interval transit time or approximately a 21% error in a velocity of 18.0 kft/sec. This kind of systematic error will not be obvious on the measured velocity log and its detection could present a problem.

P wave Arrival Time

To determine the arrival times of the P wave more precisely we propose a two step method: 1) event detection by triggering on the the first amplitude above a threshold level, and 2) fine adjustments of the detected events by a waveform correlation scheme.

In the first step of the event detection algorithm the user defines a set of threshold detection levels, one for each source/receiver pair, at the beginning of the processing. The values are selected via an interactive graphics terminal which displays the first set of waveforms. These values are usually chosen as the difference between the background noise level and halfway up the first cycle of the P wave. The user defines a time window on each record in which to search for the P wave. For subsequent traces these windows automatically follow the determined P wave arrivals. The first point of the signal to break above the threshold level on each record is identified as a possible P wave event.

The second step of the arrival time determination performs a semblance correlation between the picks determined above. Semblance is used because it discriminates against amplitude differences as well as signal shape. The amplitude of the P waves is expected to be different than the noise background. However, since the receivers are tuned to the same bandwidth as the sources, noise may have the same spectral characteristics as P waves. Any statistic that normalizes the amplitude information, such as cross correlation, will produce good correlation values for waveforms with drastically different amplitudes. Semblance will preserve the amplitude and waveform information and discriminate between low level noise and the generally larger P waveform.

After the P arrivals are identified on all four records, a fine adjustment is made on common source pairs by using the semblance cross correlation. This adjustment is accomplished for a common source pair by selecting a small window around the picked waveform on the first record and correlating it against a larger window around the picked arrival on the second record (shown in Figure 9a). The largest correlation value and its associated lag are recorded. The process is then reversed by selecting a small window around the picked arrival on the second record and correlating it against a large window centered around the picked arrival on the first record, as shown in Figure 9b. The largest value for this correlation is then compared with the largest value for the

previous correlation. The larger of these two correlation values identifies the superior pick on these two records. The lag associated with this largest value is then used to adjust the arrival time of the inferior pick, shown in Figure 9c. This process not only makes fine adjustments of the arrival times but also removes bad picks associated with uncorrelated changes in the background noise level.

If the algorithm finds a noise spike in the event detection stage, an inferior value of the semblance statistic will occur in the waveform correlation stage. The problem is to determine a significant value of coherent energy across the receivers. A 80% confidence level of the semblance statistic is 0.7 determined for two receivers and a signal bandwidth of 20 kHz. If two noise signals are analyzed with band limited spectra there is a 80% certainty that their semblance value will be less than 0.7. If the correlation values fall below this level, or if unreasonable velocities are calculated the program requests different threshold levels.

The effect of the sampling interval on the velocities measured is significant. An error in the arrival times of 5 μseconds (the selected sampling increment of the system) at velocities of 20.0 kft/sec, 10.0 ft/sec, and 5.0 kft/sec, would result in errors in the velocity estimates of 5.2%, 2.6%, and 1.2% respectively. Since the system is band limited and sampled adequately, to prevent aliasing the higher resolution of the data can be reconstructed by interpolating between the sampled values. The best resolution was obtained by interpolating between the points of the semblance correlation function. This gives the true peak of the correlation of the two P waveforms and eliminates the necessity of increasing the storage capacity and computation time to interpolate the original waveforms. A sync interpolator was used on the data to reduce the coarseness of the velocities determined.

Common source velocities

A velocity is obtained from common source pairs by calculating the moveout between the two receivers sharing the same source. This method determines two P velocities for each tool position. These velocities will be the same unless there is an increasing velocity gradient away from the borehole wall.

An analysis of fourteen traces from the synthetic suite of data yields a remarkably close reproduction of the model parameters. The average bias between the model velocities and the measured velocities is −0.23%, whereas the standard deviation was only 0.63%. Random noise with the same relative spectral amplitudes as the source was added to the limestone synthetics. Enough noise was added to reduce the peak signal to RMS noise level from 18db to 6db. Even here the average bias is only −1.8% and the standard deviation was 2.8%. These results are considered to be a satisfactory test of the velocity determining scheme.

The average of the two velocities obtained using this method on data from 200 feet of a sandstone/shale sequence is shown in Figure 10a. A width of 150μseconds was used for the smaller correlation window. The spatial resolution of this method is the receiver spacing of two feet. The P wave arrivals are successfully tracked and produce consistently reasonable

velocities.

Compensated velocities

Sonde tilt and washouts introduce errors into the common source velocities. In conventional borehole compensated sonic logging one source is placed at the top and one at the bottom of the sonde. Two receivers in the middle of the sonde detect the moveout of the P wave from each source firing. These moveouts are averaged to obtain a borehole compensated log which attempts to reduce the error caused by the tilt and washouts. The tool design of Schlumberger's SLS-TA sonde does not allow direct borehole compensation.

In order to correct for these errors interchangeability of the source and receiver is used to effect borehole compensation. The assumption of interchangeability is based on two observations. First, since the waveforms from common receiver pairs have correlation values similar to those of the common source pairs, the source waveforms appear to be quite similar in shape. Second, static time shifts between the source firing times can be removed. The average difference in the arrival times of R2 and R3 is calculated over a large depth interval, and this average time shift is subtracted from the R1 and R2 arrival times. Temporal changes in the firing times, if they exist, cannot be removed.

A pair of tool positions are at compensating depths when the two receivers of the first tool positions are located at the same depth as the two sources of the second position. to obtain effective borehole compensated velocities the moveouts between common receiver pairs are calculated using semblance. These delays are averaged with the common source delays from the appropriate compensating tool depths, as shown in Figure 11. Two velocities are determined with this method, one from the near "source," and one from the far "source."

A borehole compensation velocity analysis of the same 200 feet of a sandstone/shale sequence is shown in Figure 10b. The velocity plot shows the average of the near and far "sources" and the common source velocity log. The compensated log has somewhat higher velocities but is generally in agreement with the common source log. Figure 10c is a comparison plot of the compensated log and of Schlumberger's Borehole Compensated (BHC) Sonic log.

S WAVE VELOCITY DETERMINATION

The S wave velocity can be determined either from the presence of a distinct S headwave arrival or from the moveout (phase velocity) of the pseudo-Rayleigh wave. The S headwave arrives at the onset of the pseudo-Rayleigh wave. As synthetic acoustic logs show it cannot be distinguished from the first cycle of the pseudo Rayleigh (Cheng and Toksöz, 1980, 1981; Tsang and Radar, 1979). Since the pseudo Rayleigh velocity, c, at the cut-off frequency is equal to the shear velocity of the formation, the measurement of either the shear arrival or the onset of the pseudo-Rayleigh wave, is a measurement of the shear velocity of the formation. When the shear velocity of the formation is less than the fluid velocity, the pseudo-Rayleigh wave will not be present. In addition, the S arrival will not be recorded since a critical refraction will not be possible.

We would like to describe and compare four methods of obtaining the shear velocity from the full waveform acoustic logs. As in the P wave method, we have interpolated the correlation functions in S wave methods 2, 3, and 4 to gain higher velocity resolutions. This could also be incorporated into method 1.

Velocity analysis (method 1)

The velocity spectral analysis described for the full waveform methods can be applied to S wave velocity determination. It is approximately 25 times slower than the other three methods investigated. Owing to cost considerations only a few depths in the 200 feet of the field data previously analyzed for the P wave velocity were analyzed with this technique. A correlation window of 150 μseconds was used. The crosses in Figure 12a are the S velocities found by this method. An additional limitation of using this method on data from a tool with closely spaced receivers is that any change in the formation between the two sources will introduce a time offset and destroy the alignment of similar wavetypes. The "?" in Figure 12a shows a depth where the analysis failed to align any coherent energy.

Geometrical correlation (method 2)

Scott and Sena (1974) propose a method to obtain the shear velocity using a scanning algorithm. It computes the expected arrival times of a shear headwave at two common source receivers given formation shear velocity, tool geometry, borehole radius, and the borehole fluid velocity. This technique assumes that the formation shear velocity is constant over the length of the tool. The recorded waveforms are windowed around these arrival times and the zero lag of the cross correlation is computed on each waveform. Once the initial high trial shear velocity is calculated the trial velocity is lowered and the process is repeated until the trial velocity drops below the borehole fluid velocity. At this point the shear velocity can be determined from the correlation values which are functions of the trial velocities. The first positive peak in the correlation function, corresponding to the highest trial velocity less than the P velocity with a good coherence, identifies the shear velocity.

We modified the method to optionally include the information about the arrival times and velocity of the P wave from the results of the methods described above to determine an accurate borehole radius estimate. Even with this modification the technique has a major drawback; any change in the formation shear velocity over the length of the tool will cause misalignment of the shear headwave energy. The algorithm cannot recover the shear velocity in this case. The application of this technique is limited to formations with velocity layers greater than 10 feet or formations with only gradually changing velocity gradients. These restrictions will usually prohibit the application of this technique to S wave velocity analysis.

The synthetic test data was analyzed using this technique to obtain an estimate of its stability. "Estimates" of the borehole geometry used are shown in Table 2. When the geometry is known precisely the technique attained the model parameters with average bias of 0.42%. When the radius was changed by −62% and 54% the average biases were 7.2% and −0.4%, respectively. Geometrical correlation does not appear to be very sensitive to the drilling fluid velocity; when this parameter was changed by 15% the average bias was less

than 0.4%. Its greatest sensitivity, as predicted, is when it encounters more than one formation velocity over the length of the tool. The effect of a velocity change within the tool length was simulated by introducing a time shift in the synthetic waveforms by an amount corresponding to the difference in travel time through an artificial layer. A modest time difference of 40 μseconds, corresponding to a 4 foot layer with a 10μsec/ft slower velocity, causes a significant average bias of 7.4%. The technique is less sensitive to a faster layer; using a 40 μsecond time advance, the average bias is only −0.18.

Figure 12b shows the results of this technique for the same 200 feet of sandstone/shale field data. A correlation window width of 175 μseconds was used with common source pairs of records. The velocities found are averaged for each tool position. The computer time required (on an IBM 370/168) to process these 400 traces was 43.2 seconds.

Cross correlation (method 3)

The third method of S wave determination is based on the cross correlation of a window containing the S arrival on one record against the next record to find the best fit. This window begins at a user specified fixed point past the P arrival which is large enough to encompass the S arrival but sufficiently small to prevent contamination by other waves. The test synthetic data was processed with this method; an average bias of 0.91% and a standard deviation of 7.06% was obtained. The errors are larger for the cross correlation than for other methods. The results on the test data are shown in Figure 11c. The computer time required to process the 400 traces was 45.6 seconds. A correlation window length of 350 μseconds was used, starting 300 μseconds past the P wave arrival time. This method is generally not stable and tends to cycle skip. Care was taken in this analysis to avoid cycle skipping. It is interesting to note that these velocities are lower than those of the other methods.

P correlated S (method 4)

Willis and Toksöz (1979) propose a method to determine S wave velocities by an initial unnormalized cross correlation of the first record (shown in Figure 13) by its respective P waveform determined by the P wave detection scheme described above. The S wave arrival is identified by a search of the correlation function for the first value approximately equal to or greater than the square of the energy of the P waveform. The ratio of the acceptable correlation value to the square P wave energy is referred to as the S/P level. A window around this arrival is cross correlated against the second record, starting with a lag corresponding to $\alpha/(1.4)$ and ending with the lag corresponding to the fluid velocity. This process is repeated for each common source pair. One velocity is determined from each common source pair, resulting in two velocities.

The unnormalized cross correlation is used to preserve the amplitude information. The "shear" arrival is expected to have the same greater amplitude as the P wave. If it is identical to the P waveform its unnormalized correlation value is the square of the P wave energy. Accordingly, if it is larger its correlation value will to be greater than the square of the P wave energy. The "shear" arrival can be located using this criteria.

This method may skip over any small amplitude S waves present in favor of a larger pseudo-Rayleigh wave. It is assumed that the P wave is similar in shape to the S wave or to the onset of the guided wave; the source spectrum is narrow band and the pseudo-Rayleigh wave train is nearly sinusoidal. Since the pseudo-Rayleigh wave arrival coincides with the shear wave arrival the calculated velocity may be the velocity of the first cycle of the pseudo-Rayleigh wave. A slight underestimation of the S wave velocity is likely since the phase and group velocity of the pseudo-Rayleigh wave is equal to the shear velocity only at the low-frequency cut-off. This technique was tested with the synthetic suite of data. The average bias is −0.19% with a standard deviation of 0.22%. An analysis of synthetic data with noise results in an average bias of −0.26% and standard deviation of 0.33%. This is well within the acceptable level of error for most applications.

The average of the common source velocities are shown in Figure 12a by the solid line for 200 feet of sandstone/shale field data previously analyzed. The computer time required was 56.4 seconds. An S/P level of 0.8 and a correlation window of 175μseconds was used to process the traces.

POISSON'S RATIO

An important parameter that can be determined through the analysis of full waveform P and S wave velocities is Poisson's ratio. Toksöz *et al.* (1976) show that it is a sensitive parameter to formation fluid content. Poisson's ratio may be calculated from the velocities by:

$$\nu = \frac{1 - 0.5\left(\frac{\alpha}{\beta}\right)^2}{1 - \left(\frac{\alpha}{\beta}\right)^2} \tag{8}$$

where ν= Poisson's ratio, α= P wave velocity, and β= S wave velocity. Figure 14 shows the Poisson's ratio profile determined from the compensated P wave and P-correlated-S S wave velocity logs. Utilizing the above equation for ν and a standard method of estimating the statistical propagation of errors, (Equation 4-5 of Bevington, 1969), it is easy to show that the standard deviation of ν, σ_ν, can be found from

$$\sigma_\nu^2 = \frac{\left(\frac{\alpha}{\beta}\right)^2 \frac{1}{\beta^2}}{\left[1 - \left(\frac{\alpha}{\beta}\right)^2\right]^2} \left[\sigma_\alpha^2 + \sigma_\beta^2 \left(\frac{\alpha}{\beta}\right)^2\right] \tag{9}$$

Where σ_α and σ_β are the standard deviation of the estimates for α and β, respectively. If we assume $\frac{\alpha}{\beta} = 1.7$ and use our estimates of $\frac{\sigma_\alpha}{\alpha} = 0.63\%$ and $\frac{\sigma_\beta}{\beta} = 0.22\%$ determined for the synthetic data, then $\frac{\sigma_\nu}{\nu} = 2.3\%$. It can be predicted as well as observed that Poisson's ratio will be subject to more noise than the measured velocities.

COMPARISON OF VELOCITIES WITH LITHOLOGY AND OTHER DATA

An important reason for determining both compressional and shear wave velocities and the associated Poisson's ratio is to infer lithology and saturation properties of the formations. In order to test this, data from three wells were analyzed and correlated with other logs. The three wells are referred to as Wells 1, 2, and 3. In all three cases the actual depth scales have been changed in order to protect the identity of the wells.

Well 1

Full waveform data from a 200 foot section of this well was used throughout this paper as the reference field data. The velocity profiles are shown in Figure 14. The data was recorded using a Schlumberger SLS-TA sonde. This tool has two transmitters at the bottom which are separated by 2 feet. At the top are two receivers which are separated from each other by 2 feet. The transmitters are isolated from the receivers by a slotted steel spacer which is 7 feet in length. The sampling interval was set at 5 μseconds.

Figure 15 shows in sign bit plot of the data from one of the receivers with a 9 foot source/receiver separation. For a particular tool depth, the record is displayed on the time axis as either dark for positive amplitudes or blank for negative amplitudes. The sign bits for records from consecutive depths of this receiver are plotted side by side. The P headwave arrival clearly stands out above the background noise at about 0.72 milliseconds. The start of the pseudo-Rayleigh wave is identified as the change in character of the log at about 1.2 milliseconds. The Stonely wave arrival is evident at about 1.85 milliseconds. Figure 16 shows a set of four waveforms from this data set at a depth of 6680 feet. Features that are difficult to identify on individual waveforms are often more clear on a sign bit display. It is also very convenient to display a large volume of data in this format.

Lithology: The zone of Well 1 studied is a sandstone shale sequence. The porosity of the sandstone is generally under 10% in the section. The nearly constant signature at the top of the sign bit plot of the data (Figure 15, depth 6750 feet to 6725 feet) is due to cable slack when the tool was resting at the bottom of the hole. As the cable was reeled up the borehole data was recorded from which the following lithology can be interpreted: from 6725 feet to 6698 feet a low porosity (less than 4%) sandstone, from 6692 feet to 6698 feet a shale, from 6692 feet to 6670 feet a sandstone with about 10% porosity, from 6670 feet to 6655 feet a clean sandstone with approximately 5% porosity, from 6655 feet to 6635 feet a shaley section, and from 6635 feet to 6550 feet a sandstone with porosity generally less than 10%. With information from the corresponding compensated neutron porosity and formation density logs it is possible to interpret gas shows or limestone cementation at 6582 feet, 6570 feet, and 6555 feet. Gas is probably unlikely, however, since this is an oil well in which pressure has been maintained.

Velocity: The velocity profiles for this data set are shown in Figure 14 along with a profile of Poisson's ratio derived from the P and S wave velocities. The P wave velocity is slightly higher in some places than the conventional Schlumberger BHC sonic log (see Figure 10c). This is probably due to the longer source/receiver offset of the full waveform data which allows greater penetration behind damaged zones around the borehole than does the shorter spacing (3-5 feet) of the BHC log. The Poisson's ratio for this data is about 0.24. The notable exceptions to this value are at depths 6710 feet, 6660 feet , and 6588 feet. It is difficult to determine the lithology at 6710 feet since it is so close to the bottom of the well. For the other two depths, where the Poisson's ratio decreases, both P and S velocities increase. A velocity increase with a low Poisson's ratio corresponds to a decrease in the porosity of the sandstone. The very low Poisson's ratio suggests either a very clean sand or gas saturation or both. This is an interesting correlation and shows the possible use of the Poisson's ratio as well as P and S velocities for inferring formation properities.

Well 2

The tool used to record the data for this well was a Schlumberger SLS-TA type tool with the same configuration as for Well 1. The slotted steel spacer was 8 feet, however, and the sampling interval was increased to 6 μseconds. The data indicated an electronic problem in the digitizer triggering circuitry during recording. The mechanism was apparently triggering early by at least 20 samples, causing the fullwave logs to begin 120 to 150 μseconds earlier than the actual source firing time.

Figure 17 shows the sign bit plot of the data from one of the receivers with a 10 foot source/receiver separation. Two representative waveforms from this data set are shown in Figure 18, one from a 10 foot waveform at a depth of 1082 feet (Figure 18a) and the other from a 10 foot waveform at 1009 feet (Figure 18b). The P headwave arrives at about 1.05 milliseconds and it is labeled P in Figure 17. Through the comparison of Figure 18 with Figure 17, the pseudo-Rayleigh wave arrival can be seen on the sign bit plot at about 1.7 milliseconds. It is labeled as R.C. on Figure 17. A distinct Stoneley wave arrival, however cannot readily be observed.

Lithology: The study zone from Well 2 has high porosity (10 - 25%) and is composed of dolomitic limestone and sandstone. The gamma ray log shows the zone to be fairly clean, *i.e.*, free from shale. Below 1020 feet the formation appears to be a dolomitic limestone which varies between 100% limestone—no dolomite, and about 50% limestone—50% dolomite. This was determined from the compensated neutron porosity and compensated formation density logs. Above 1020 feet it appears to be a sandstone with about 10% carbonate. It is also possible that it contains gas, while below 1020 feet it is probably water saturated.

Velocity: Figure 19 shows the velocity profiles and α/β ratio determined from the full waveform data for Well 2. The velocities presented in Figure 19 have not been borehole compensated because it would have resulted in a loss of the information from the the zone above 1013 feet. There is good agreement between our full waveform α velocities and the standard BHC sonic log. Again the full waveform velocities are slightly higher in some places than velocities obtained from the corresponding sonic log.

This paper assumes a velocity contrast where $\alpha>\beta>\alpha_f$. When this assumption is valid, the first part of the pseudo-Rayleigh wave is most sensitive to the formation shear velocity. When the shear velocity drops below the fluid velocity the pseudo-Rayleigh wave is not excited. It is difficult to ascertain the exact drilling fluid velocity. Cheng and Toksöz (1981) used 6.0 kft/sec to match their acoustic waveform data. In this zone the formation shear velocity is very close to the fluid velocity.

The α/β ratio plot shows values generally $\geq$1.8 for depths below 1020 feet which is indicative of limestones and dolomites. Above 1020 feet the α/β ratio drops due to a decrease in P wave velocity. The combined behavior of α, β, and α/β suggests that the formation above 1020 feet is most likely gas saturated.

Well 3

The data for this well were collected using a Schlumberger SLS-SB tool. It is identical in design to the SLS-TA used in Well 2 where the slotted spacer was 8 feet. The sampling interval was set at 6 μseconds and again, the digitizer triggering problem is apparent on this data set. Figure 20 shows the sign bit plots for the data from the section of this well which was used to compare with the core measurements. The P headwave is labeled P and the pseudo-Rayleigh wave is labeled R-C.

Lithology: The section is fairly uniform and has a porosity between 1% and 1.5%. The uniform nature of the section is demonstrated by the coherency of the sign bit plot in Figure 20.

Velocity: Figure 21 shows the velocity profile and α/β ratio determined from the full waveform data. The solid lines show the velocities which have not been borehole compensated. The dashed lines show the borehole compensated estimates. Both the velocities and the α/β ratio is fairly uniform over the whole section. The α/β ratio of about 1.8 is typical of carbonates. The P wave velocity of about 14.5 kft/sec is too low for non porous limestone and consistent with shaliness. The slight velocity increase at 1016 feet depth may be due to a decrease in shaliness.

DISCUSSION

In this paper different methods of determining P and S wave velocities from full waveform acoustic logs were examined and examples of the utilization of velocities and velocity ratios were given. P and S wave velocities are important measurements with wide uses for exploration and formation evaluation. In

addition to absolute values of velocities, the changes in their ratios are very sensitive to even subtle changes in formation properties. The accuracy of the velocity ratios depends both on the accuracies of P and S wave velocities. Since the S wave velocity is the more difficult of two velocities to determine much effort was devoted to finding effective methods for S velocity determination.

The method of picking P wave velocities based on threshold detection and semblance correlation of the arrival picks works very well. Many other schemes were examined (although not presented) using changes in background noise levels, changes in the period of the noise, and correlation with reference waveforms. All of these other techniques displayed significant failure rates when presented with the nearly monochromatic signals present on the logs. Correlation provided us with a way of finding the moveout between records.

The comparison of the full waveform compensated P velocities and those of a standard BHC sonde generally show good agreement between the two logs. It has been documented that long spaced sonic tools measure deeper into the formation and record faster velocities than BHC tools (Thomas, 1977; Goetz *et al.*, 1979). The compensated velocities determined are slightly greater than the BHC log velocities in all cases tried. No consistent difference is found between the near and far compensated velocities, however, the difference in spacing is only 2 ft in the data analyzed. In order to perform the borehole compensation it is necessary to rely upon an accurate determination of relative depth. If the depth is not accurate the proper compensating tool positions cannot be aligned correctly. A more reliable method would be to use the BHC tool design for the full waveform sonde.

There is no universal method to determine shear wave velocity. If formation shear velocity is less than borehole fluid velocity, no refracted shear wave exists and it is necessary to determine the S wave velocity from the phase velocity of Stoneley waves. If the tool has a large number of receivers, then a velocity analysis approach either in the frequency or time domain would be a stable, although a computationally slow method. The use of the guided wave (pseudo-Rayleigh or Stoneley) phase velocities works well when the sonde has a broad frequency response.

For cases where shear wave velocities are higher than the borehole fluid velocity the P correlated S method works well. In the correlation, it skips over the P wavetrain and locates the S wave or the beginning of the pseudo-Rayleigh wave. This speeds up the computation and cuts down on "miscorrelation." By examining P and S arrival times, it is found that the onset of "S" energy picked by hand coincides very closely with S wave picks determined by this method. In addition, the P correlated S method had the smallest errors in the estimates of the synthetic data.

TABLE 1

Model parameters for synthetic suite of full waveform acoustic logs. α and β are the formation P and S velocities, α_f is the borehole fluid velocity (all in kft/sec). Q_α, Q_β, and Q_f are the dimensionless quality factors (Q^{-1} = attenuation) for the formation P and S wave and the borehole fluid compressional wave, respectively. ρ_r and ρ_f are the formation and fluid densities in g/cc. Z is the source receiver offset in feet. r is the radius of the borehole in inches. The source for all cases is tuned at 13 kHz, r = 2.6, and Z=8 and 10.

Limestone Models

For all cases: Q_p=100, Q_s=65, Q_f=20, ρ_r=2.3, ρ_f=1.2, and α_f=5.2.

Model	α	β
a)	19.5	10.5
b)	19.305	"
c)	19.11	"
d)	18.915	"
e)	18.525	"
f)	19.5	10.395
g)	"	10.29
h)	"	10.185
i)	"	9.975

Shale Models

For all cases: Q_p=60, Q_s=40, Q_f=20, ρ_r=2.0, ρ_f=1.2.

Model	α	β	α_f
j)	10.5	6.	5.2
k)	"	"	5.0
l)	10.395	"	5.2
m)	10.185	"	"
n)	9.975	"	"

TABLE 2

Geometrical correlation sensitivity study on the synthetic limestone data. μ and σ are the average bias and standard deviation between model and the measured shear velocities in percent.

Description	μ	σ
1. Correct estimates	−0.42	0.62
2. Change radius −62%	7.15	9.80
3. Change radius 54%	−0.36	0.53
4. Change fluid velocity 15%	0.36	1.09
5. Delay 40 μsec	7.40	10.22
6. Advance 40 μsec	−0.20	0.58

REFERENCES

Bevington, P.R., 1969, Data Reduction and Error Analysis for the Physical Sciences: McGraw-Hill, New York.

Brune, J., Nafe, J., and Oliver, J., 1960, A simplified method for analysis and synthesis of dispersed wave trains: J. of Geophys. Res., vol. 65, no. 1, pp. 287-304.

Cheng. C. H., and Toksöz, 1980, Modeling of fullwave acoustic logs, Paper J, 21st Ann. Log. Symp. Trans. of Soc. of Prof. Well Log Analysts, Lafayett, LA.

_____, 1981, Elastic wave propagation in a fluid-filled borehole and synthetic acoustic logs: Geopysics, vol. 46, pp. 1042-1053.

_____ ,1982, Generation, propagation and and analysis of tube waves in a borehole: Trans. of 23rd Ann. Log. Symp. of the S.P.W.L.A., July 6-9, Paper P, Corpus Christi, TX.

Cheng, C.H., Toksöz, M.N., and Willis, M.E., 1981, Velocity and attenuation from full waveform acoustic logs: Trans. SPWLA 22nd Ann. Logging Symp., Paper O. Mexico City, Mexico.

Cheng, C.H., Toksöz, M.N., and Willis, M.E., 1982, Determination of in situ attenuation from full waveform acoustic logs: J. Geophy. Res. v.67, pp. 5257-5291. in press.

Goetz, J.F., Dupal, L., and Bowler, J., 1979, An investigation into discrepancies between sonic log and seismic check shot velocities: A.P.E.A. (Australian Petrol. Explor. Assoc.) Journal, vol. 19, pt. 1, pp. 131-141.

Levinson, N., 1947, The Wiener RMS (root mean square) error criterion in filter design and prediction: Journal of Mathematics and Physics, vol. XXV, no. 4, pp. 261-278.

Roever, W., Rosenbaum, J., and Vining, T., 1974, Acoustic waves from an impulsive source in a fluid-filled borehole: J. Acous. Soc. Am., vol. 55, no. 6, (June), pp. 1144-1157.

Scott, J.H., and Sena, J., 1974, Acoustic logging for mining applications: 15th Ann. Logging Symp. of Soc. of Prof. Well Log Analysts.

Taner, M.T. and Koehler, F., 1969, Velocity spectra - digital computer derivation and applications of velocity functions: Geophysics, vol. 34, no. 6, pp. 859-881.

Taylor, S.R., and Toksöz, M.N.,1982, Measurement of interstation phase and group velocities and Q using Wiener filtering: Bul. of Seism. Soc. of Am., vol. 72, no. 1, pp. 73-91.

Thomas, D.H., 1977, Seismic applications of sonic logs: SPWLA 5th European Log. Symp., Paris, France.

Toksöz, M.N., Cheng, C.H., and Timur, A., 1976, Velocities of seismic waves in porous rocks: Geophysics, vol. 41, no. 4, pp. 621-645.

Tribolet, J.M., 1977, A new phase unwrapping algorithm: IEEE Trans. of Acoustic, Speech and Signal Process., vol. ASSP-25, no. 2.

Tsang, L. and Rader, D., 1979, Numerical evaluation of transient acoustic waveform due to a point source in a fluid-filled borehole: Geophysics, vol. 44, no. 10, pp. 1706-1720.

Willis, M. E., 1983, Seismic velocity and attenuation from full waveform acoustic logs: Ph.D. Thesis, Massachusetts Institute of Technology, Cambridge, MA.

Willis, M.E. and Toksöz, M.N., 1979, Velocity and attenuation determination from digital full wave sonic logs: Paper R-19, presented at the 49th Annual International Meeting of S.E.G., New Orleans, LA.

_____, 1982, Automatic P and S velocity determination from full waveform digital acoustic logs: Submitted to Geophysics.

Winbow, G.A., 1980, How to separate compressional and shear arrivals in a sonic log: Presented at the 50th Ann. Intl. Meeting of Society of Exploration Geophysicists, Houston, TX.

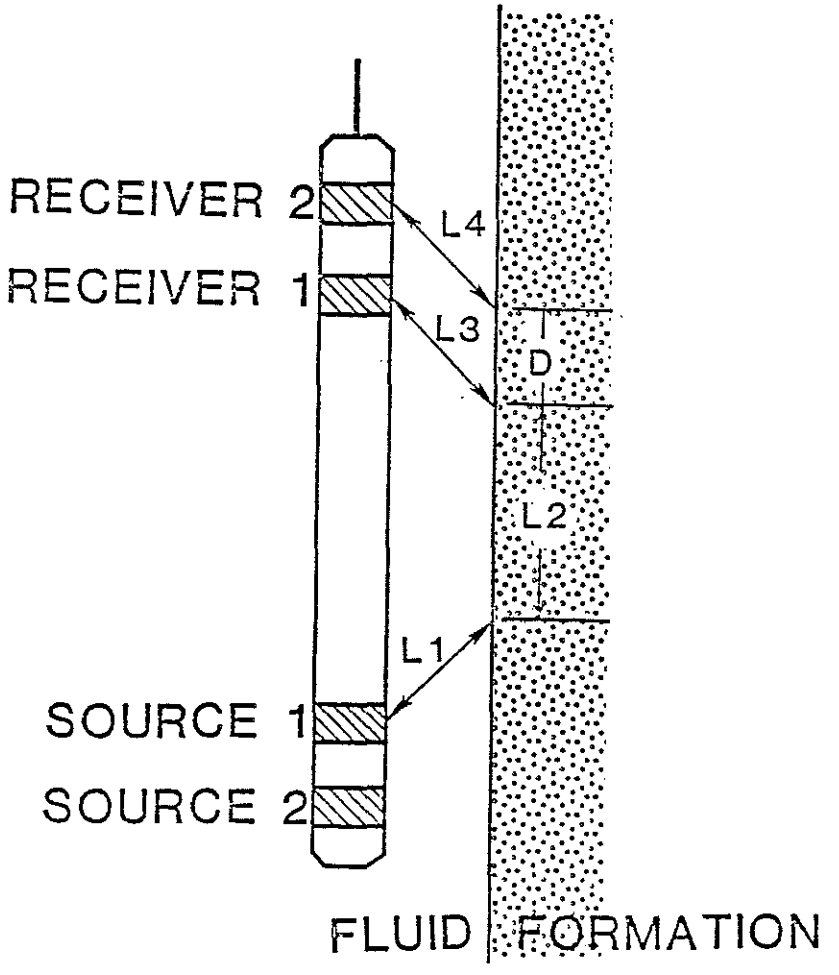

Figure 1. Schematic of the borehole. The travel paths of the headwaves through the system are also shown. L1 denotes the path of the headwave from the source to the formation. L2 denotes the path of the headwave in the formation. L3 denotes the path of the headwave from the formation to the near receiver. D denotes the additional path in the formation that the ray to the far receiver takes. L4 denotes the path of the headwave from the formation to the far receiver in the fluid.

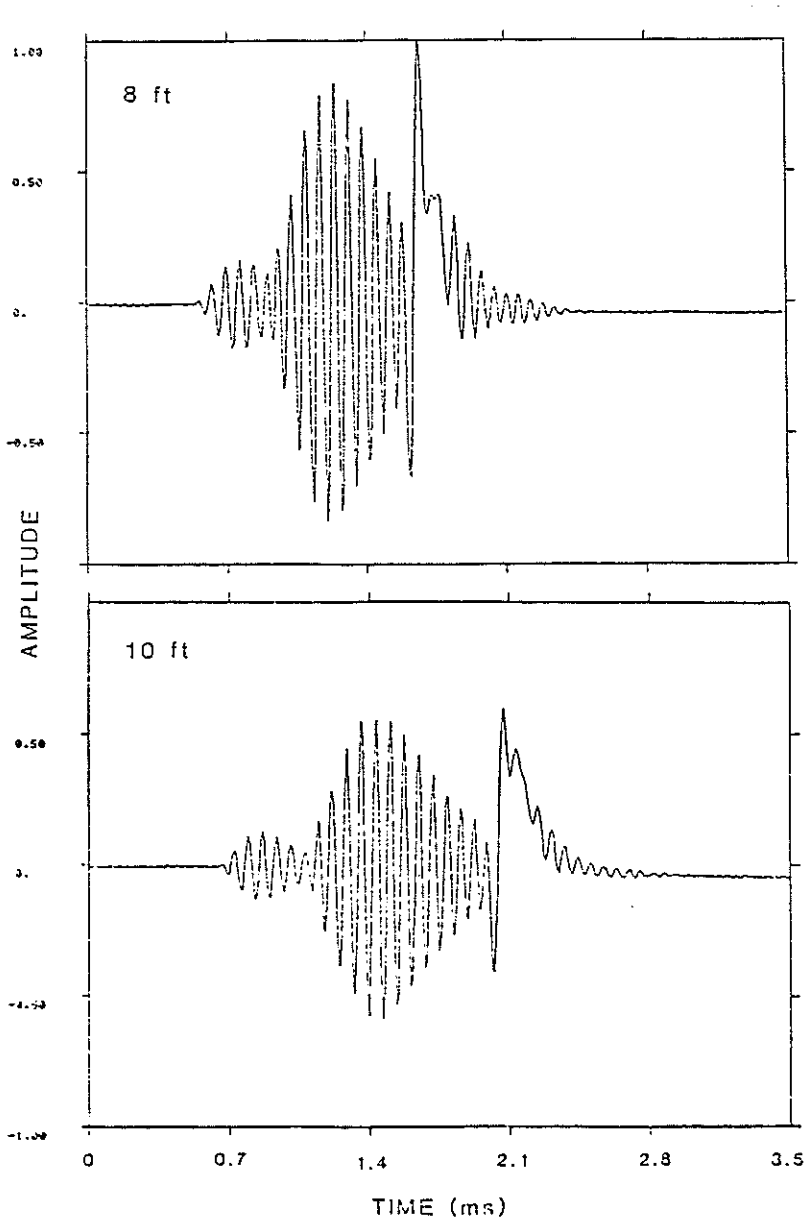

Figure 2 The near and far (R1 and R2) synthetic waveforms for model a of Table 1. The source receiver separation for the waveforms are 8 and 10 feet.

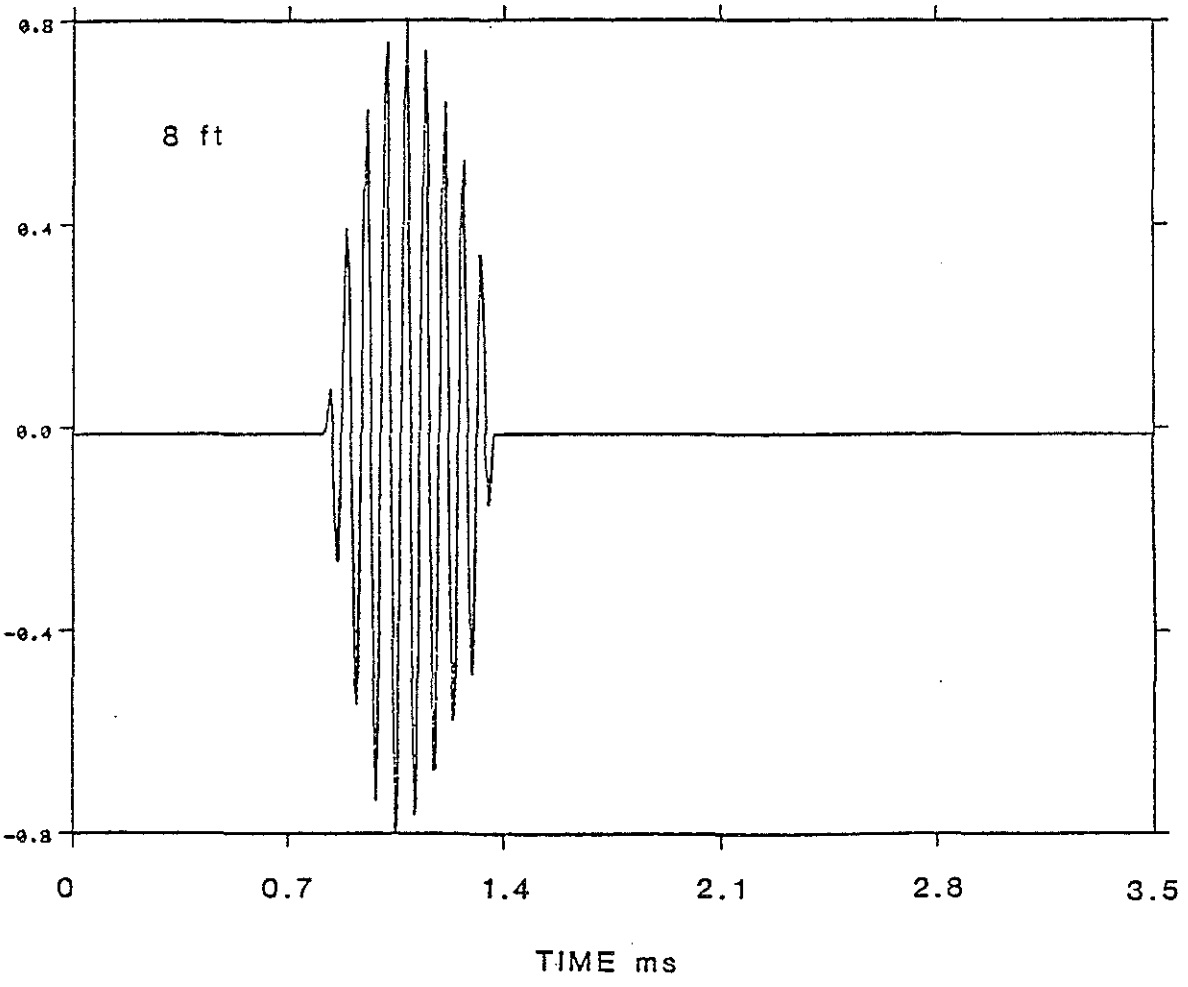

Figure 3a. The windowed portion of the R1 record shown in Figure 2. A 70 microsecond cosine taper was applied to the edges of the window selected.

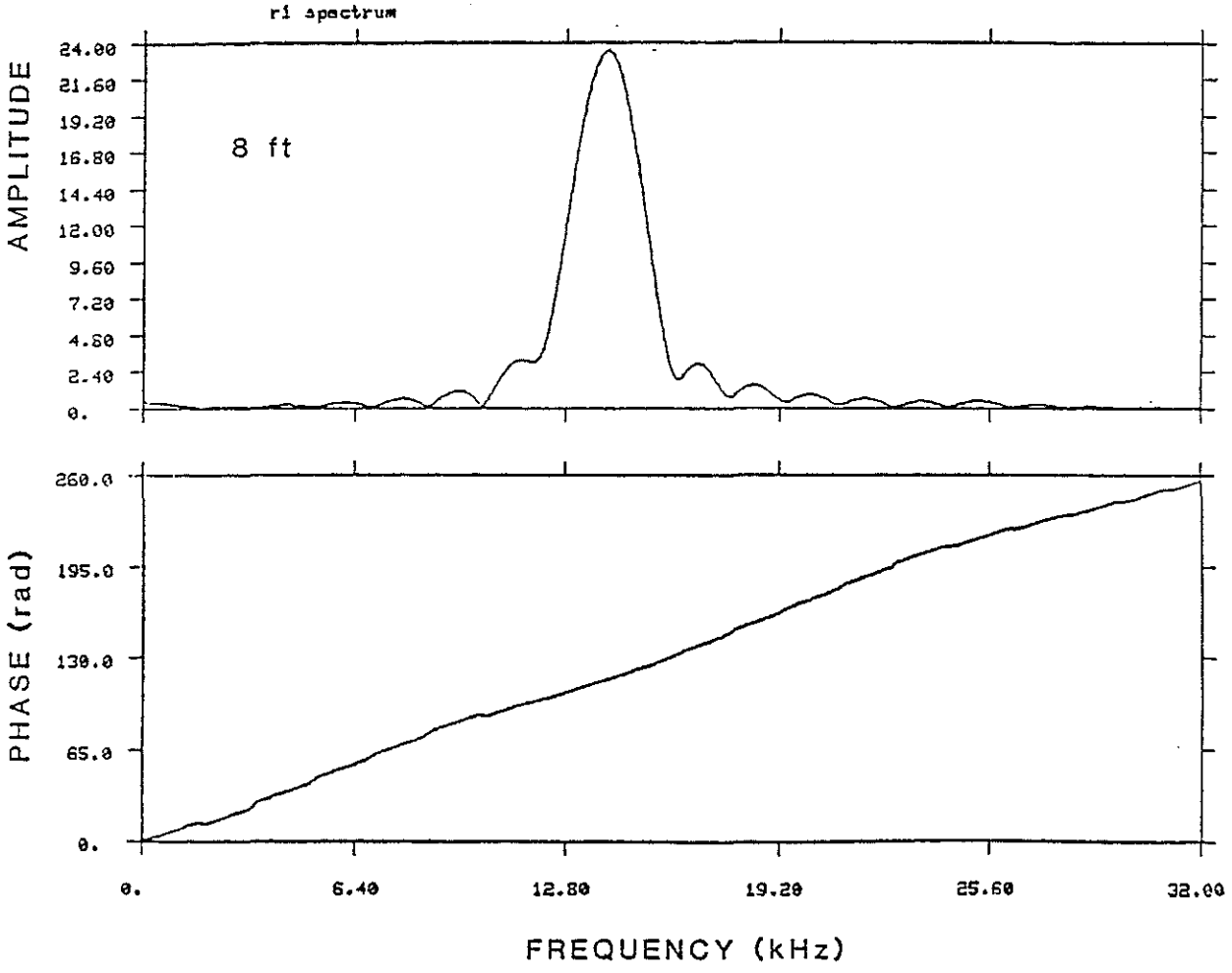

Figure 3b. The amplitude and phase spectra for the windowed synthetic waveform shown in Figure 3a.

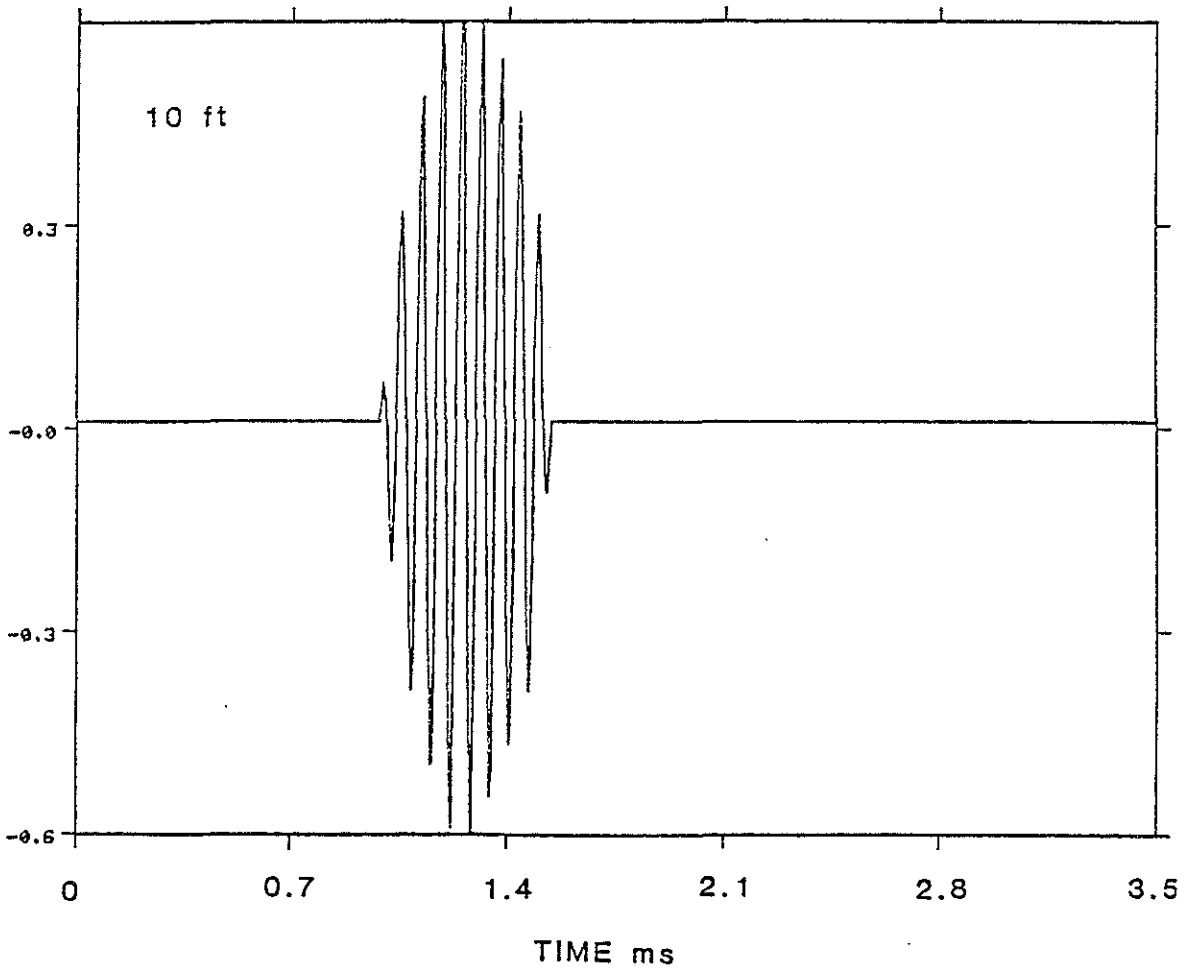

Figure 4a. The windowed portion of the R2 record shown in Figure 2. A 70 microsecond cosine taper was applied to the edges of the window selected.

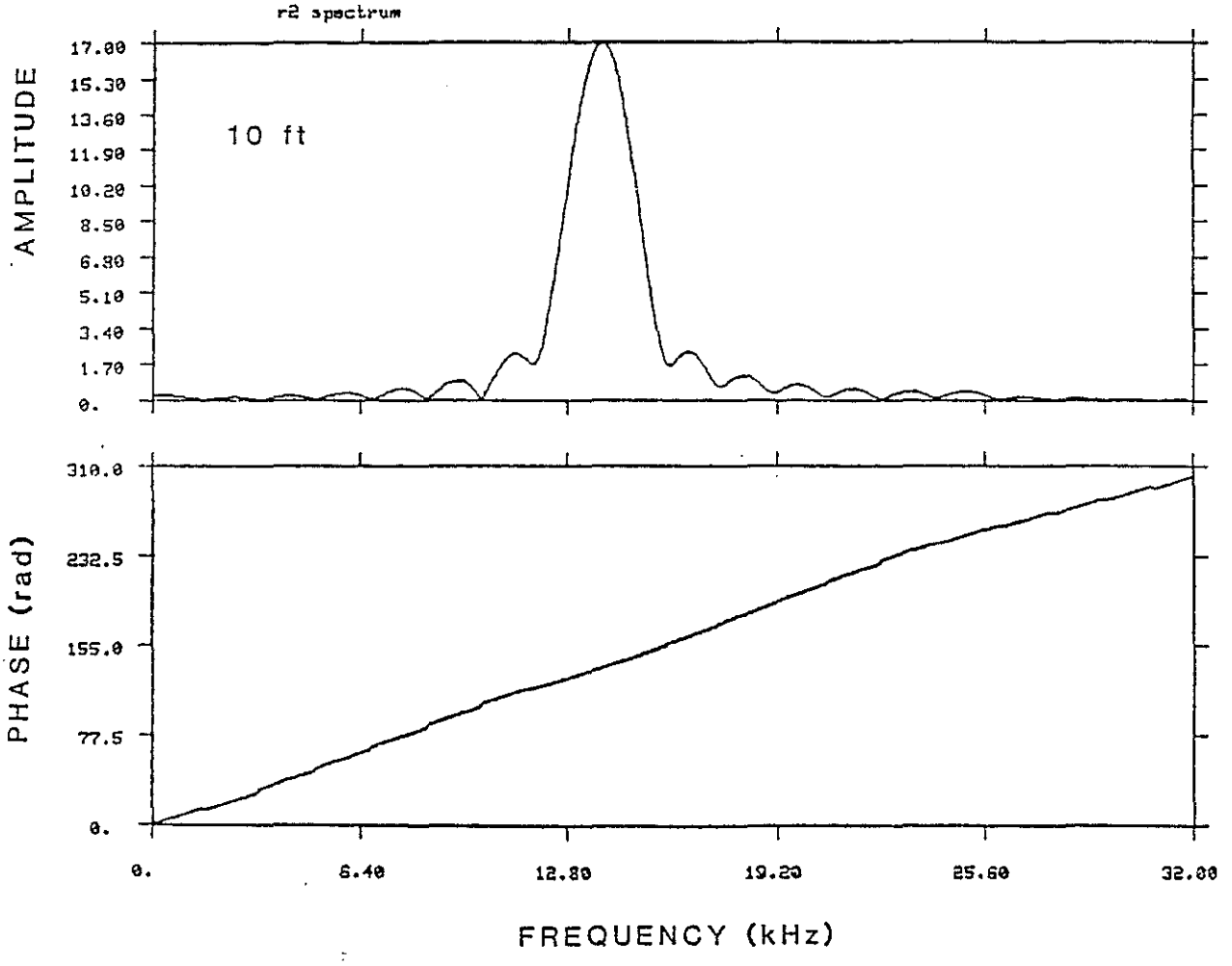

Figure 4b. The amplitude and phase spectra for the windowed synthetic waveform shown in Figure 4a.

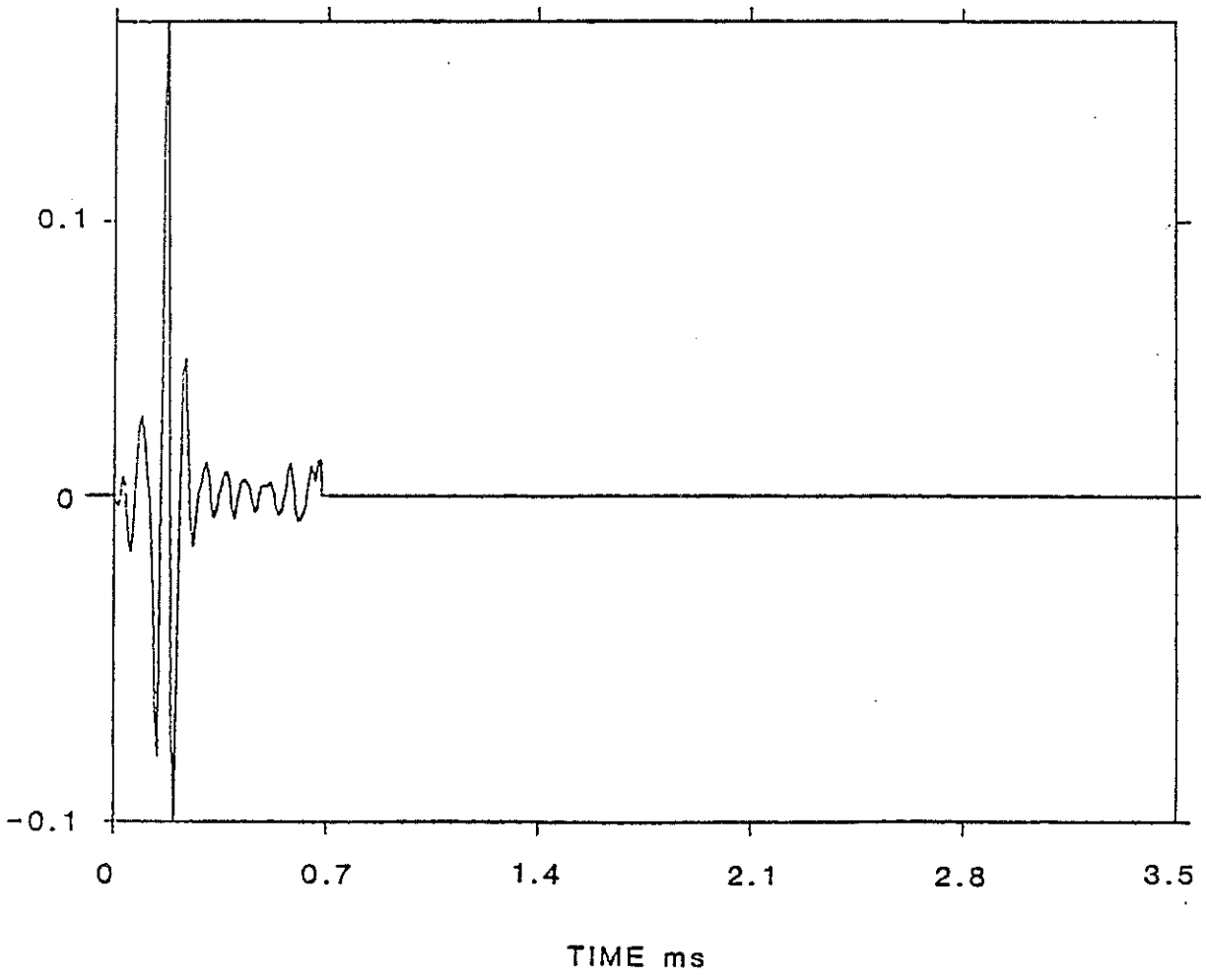

Figure 5a. The Wiener filter constructed from the waveforms in Figures 3a and 4a. The filter length was chosen as 100 points.

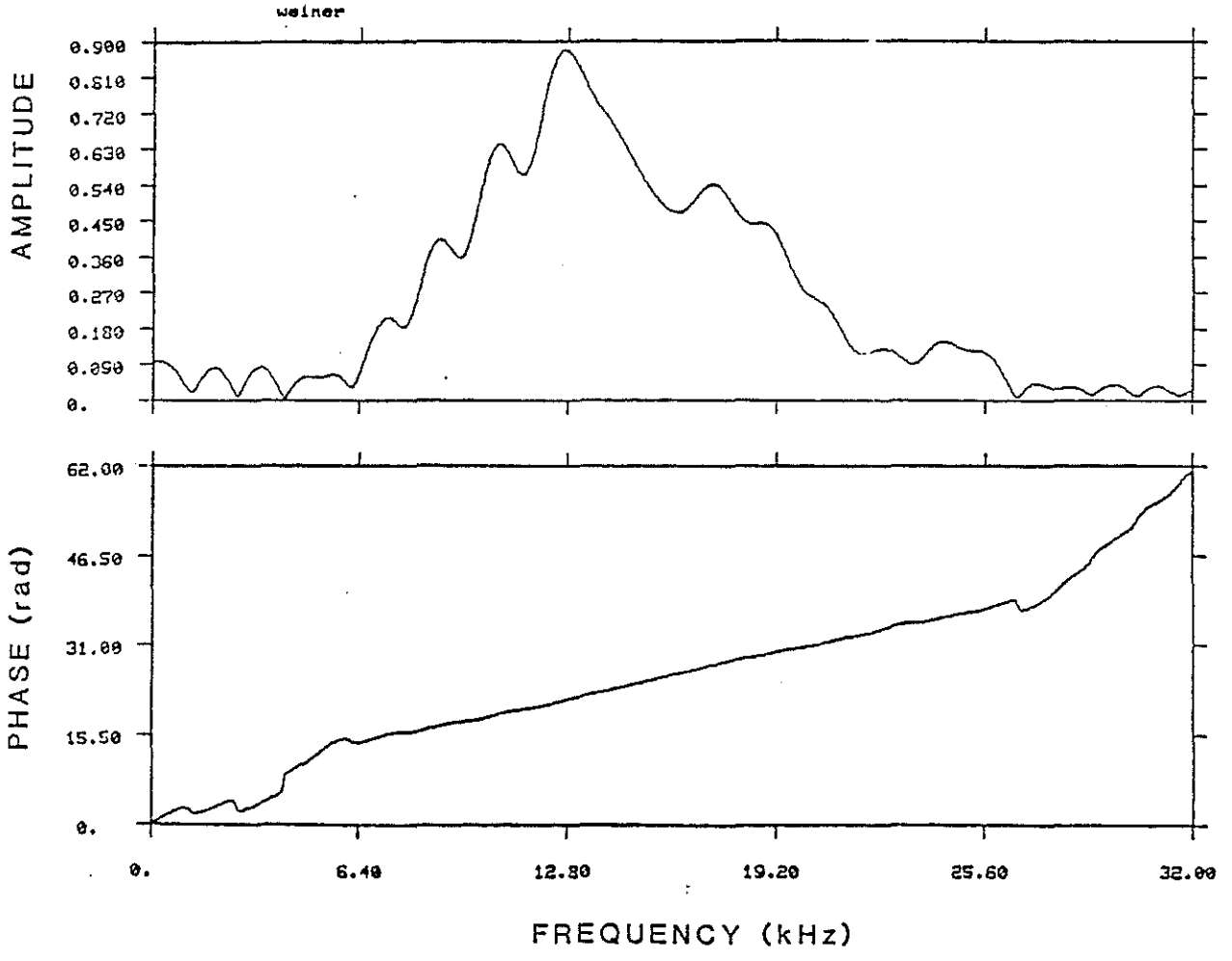

Figure 5b. Amplitude and phase spectra of the Wiener filter shown in Figure 5a.

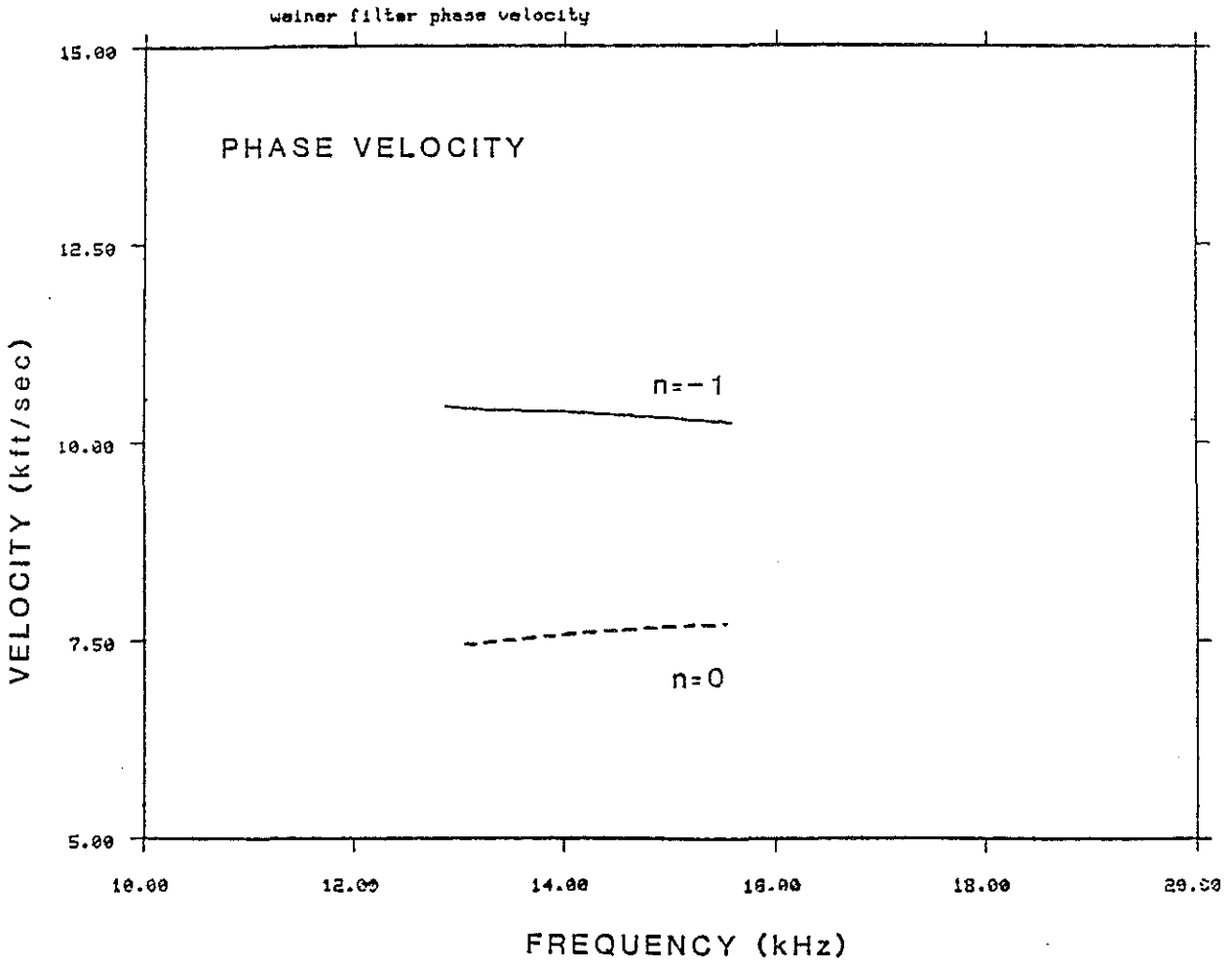

Figure 6. The phase velocity computed from the phase spectrum of the Wiener filter shown in Figure 5 using two values of n. (n is the constant which must be determined.) The solid line is for $n=-1$. The dashed line is for $n=0$. This demonstrates that the value of n is well constrained.

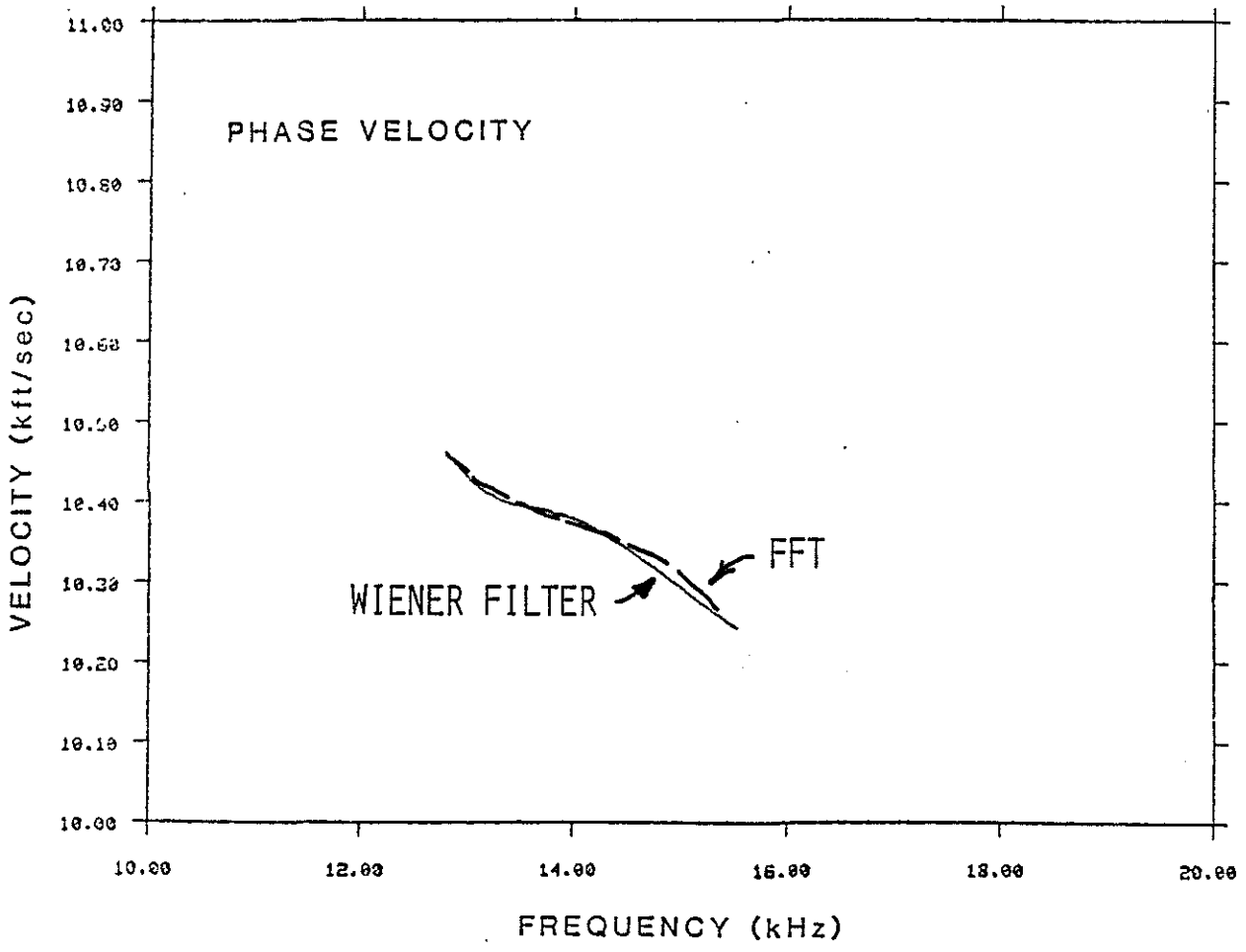

Figure 7. The dashed line shows the phase velocity of the windowed synthetic waveforms in Figures 3 and 4 using equation 6. This utilizes the Fourier phase spectra of both of the waveforms. The value of n was taken as -1. The solid line shows the phase velocity using the Wiener filter with a value of n as -1.

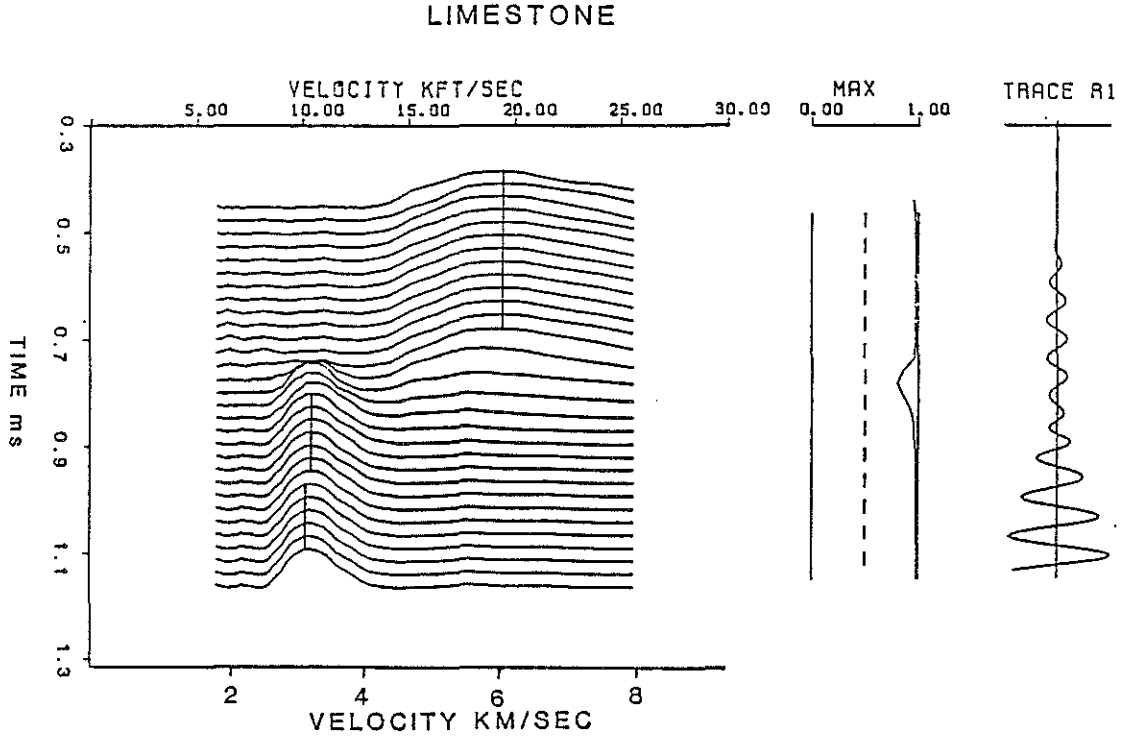

Figure 8a. a) Velocity analysis for five synthetic limestone records with parameters listed in Table 1.

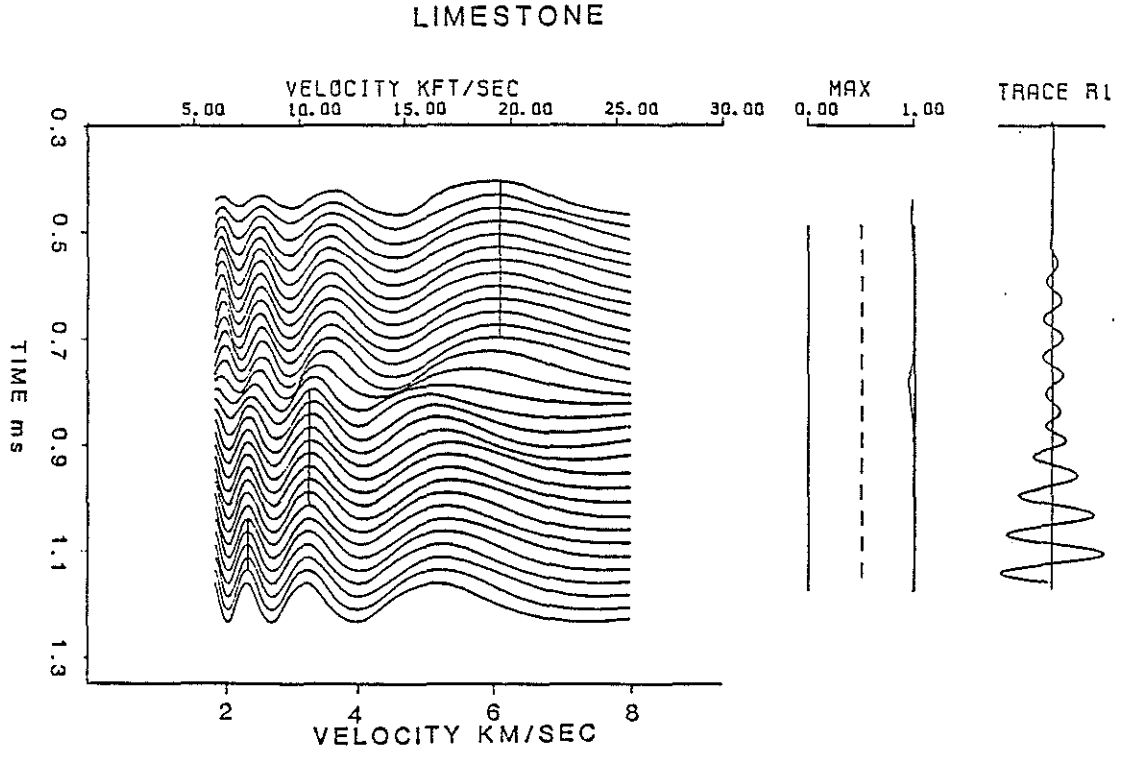

Figure 8b. Velocity analysis for two (8 and 10 ft source/receiver offset) of the five records used in a.

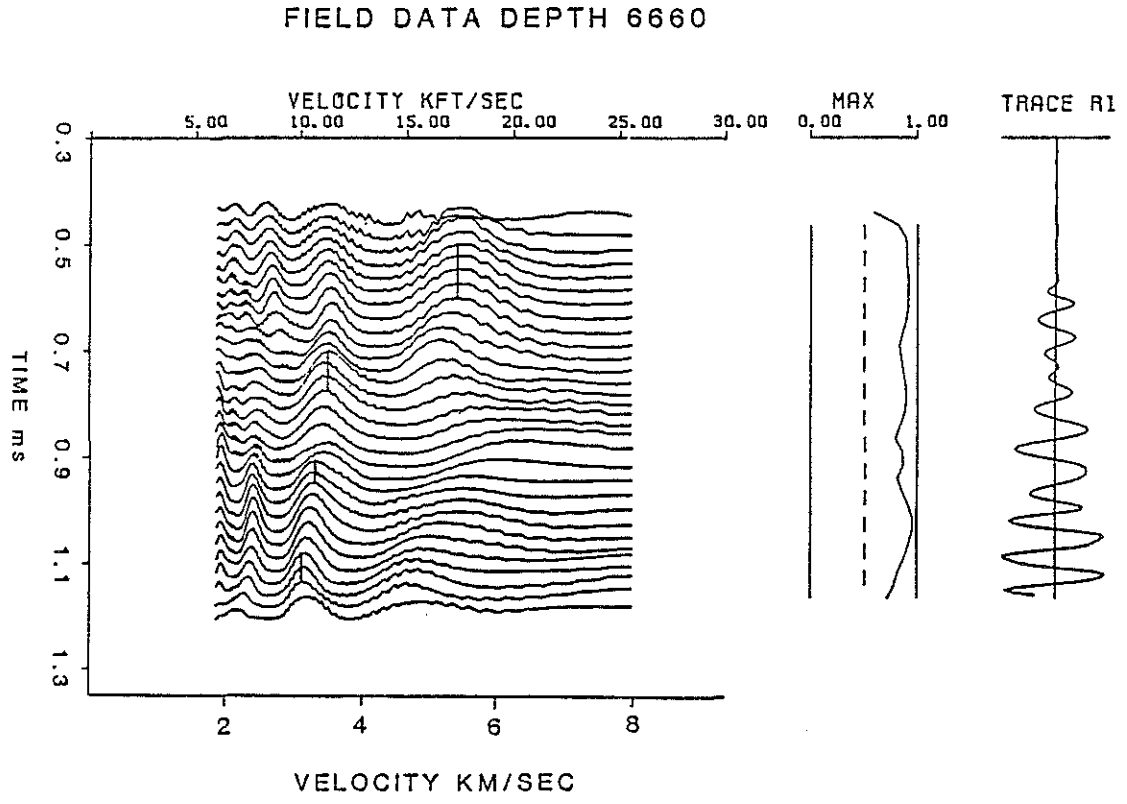

Figure 8c. Velocity analysis of four field data records using semblance. The amplitude of each trace is the semblance value as a function of velocity and time.

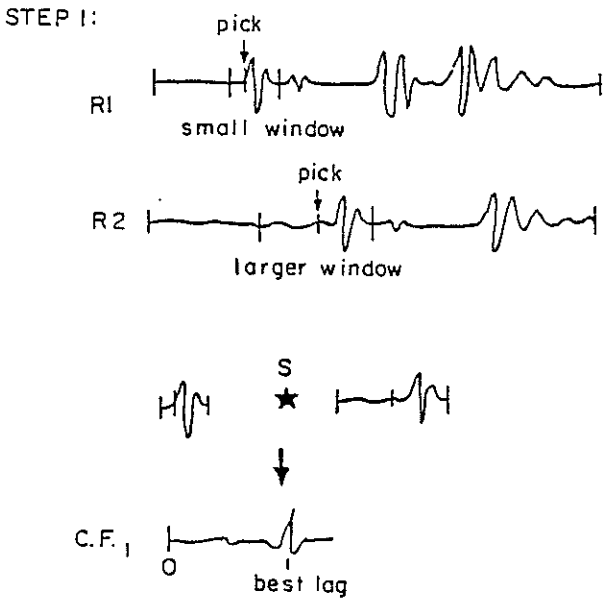

Figure 9a. Schematic drawing showing the fine adjustment of picked arrivals on records R1 and R2 by semblance cross correlation. A small window around the arrival on R1 is correlated with a larger window around the arrival on R2.

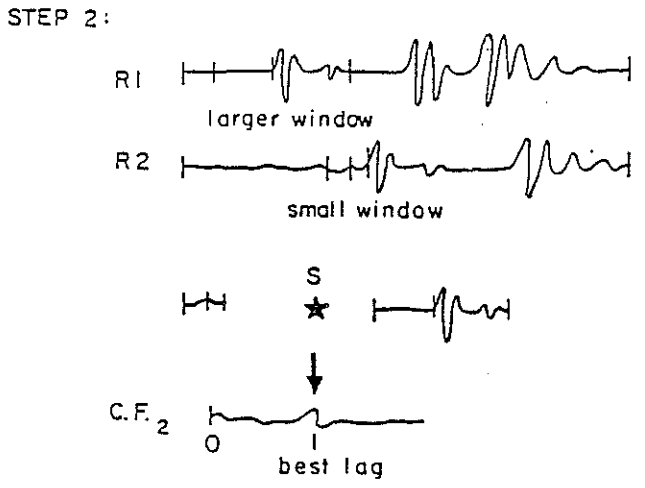

Figure 9b. The process is then reversed; a small window of R2 is correlated with a larger window of R1.

STEP 3:

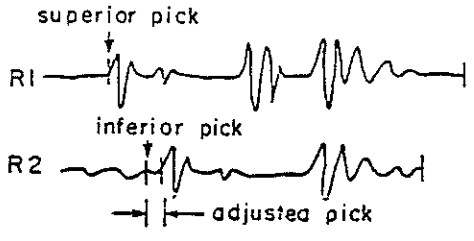

Figure 9c. The correlation function with the highest value is chosen which indicates the superior pick. The inferior pick is then adjusted to fit the lag corresponding to the superior correlation function. S star denotes a semblance cross correlation; C.F. denotes correlation function.

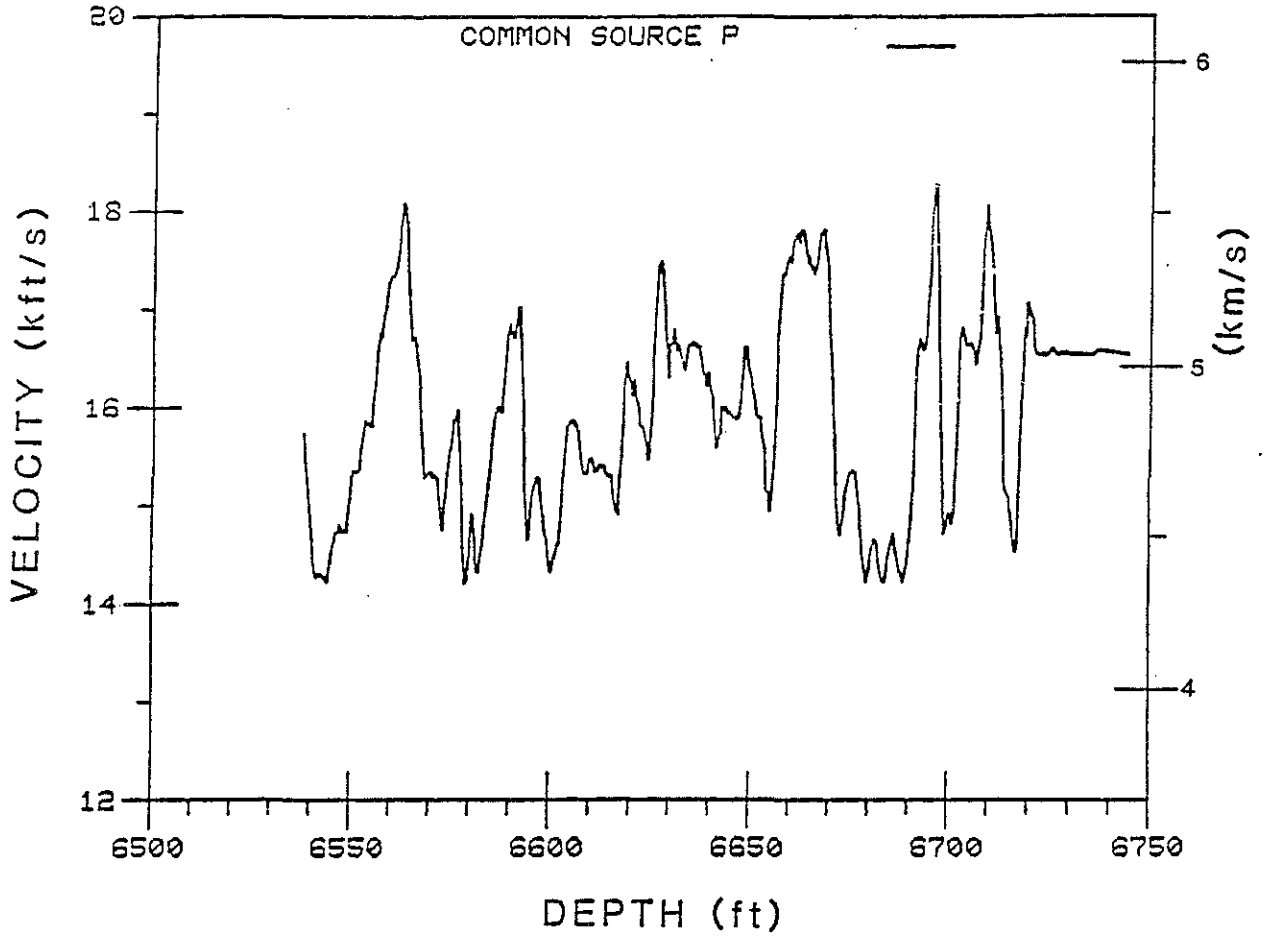

Figure 10a. Well log for a sandstone/shale sequence showing common source velocities.

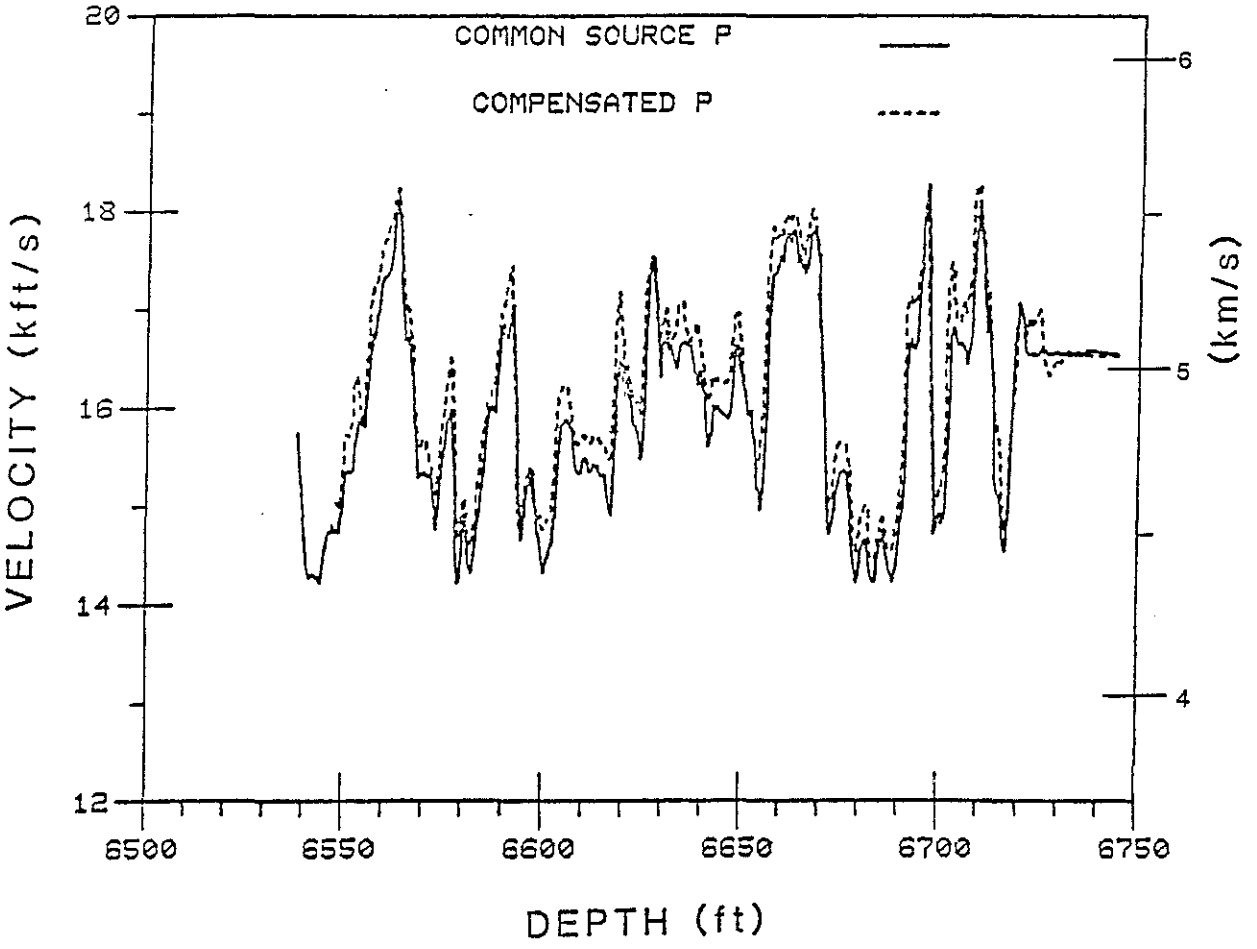

Figure 10b. Well log for a sandstone/shale sequence showing common source and compensated velocities.

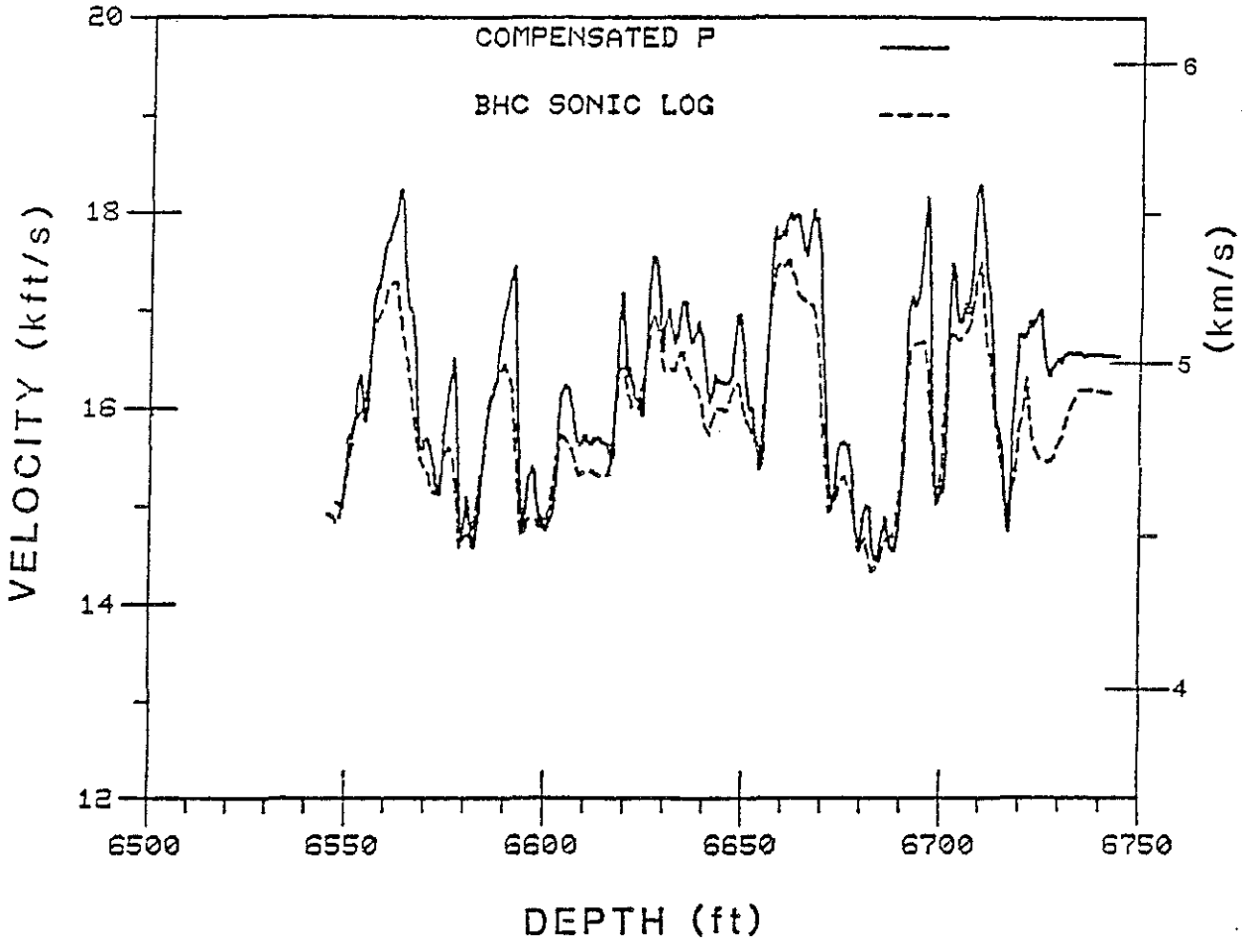

Figure 10c. Well log for a sandstone/shale sequence showing compensated velocities and a conventional BHC log.

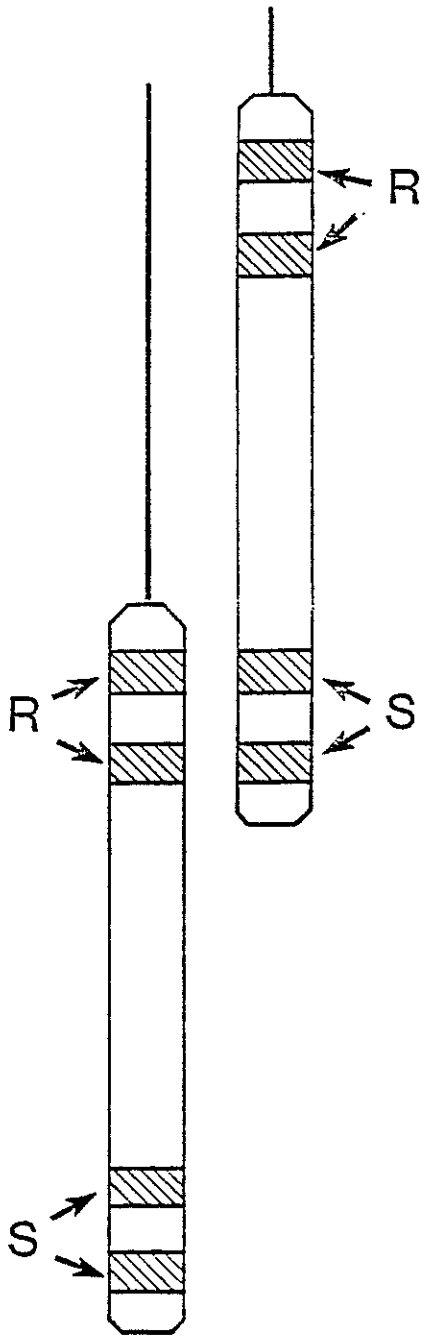

Figure 11. Two tool positions used to simulate borehole compensation. The common source velocities from the lower tool position are added to the common receiver velocities from the upper tool position. (S and R denote sources and receivers.)

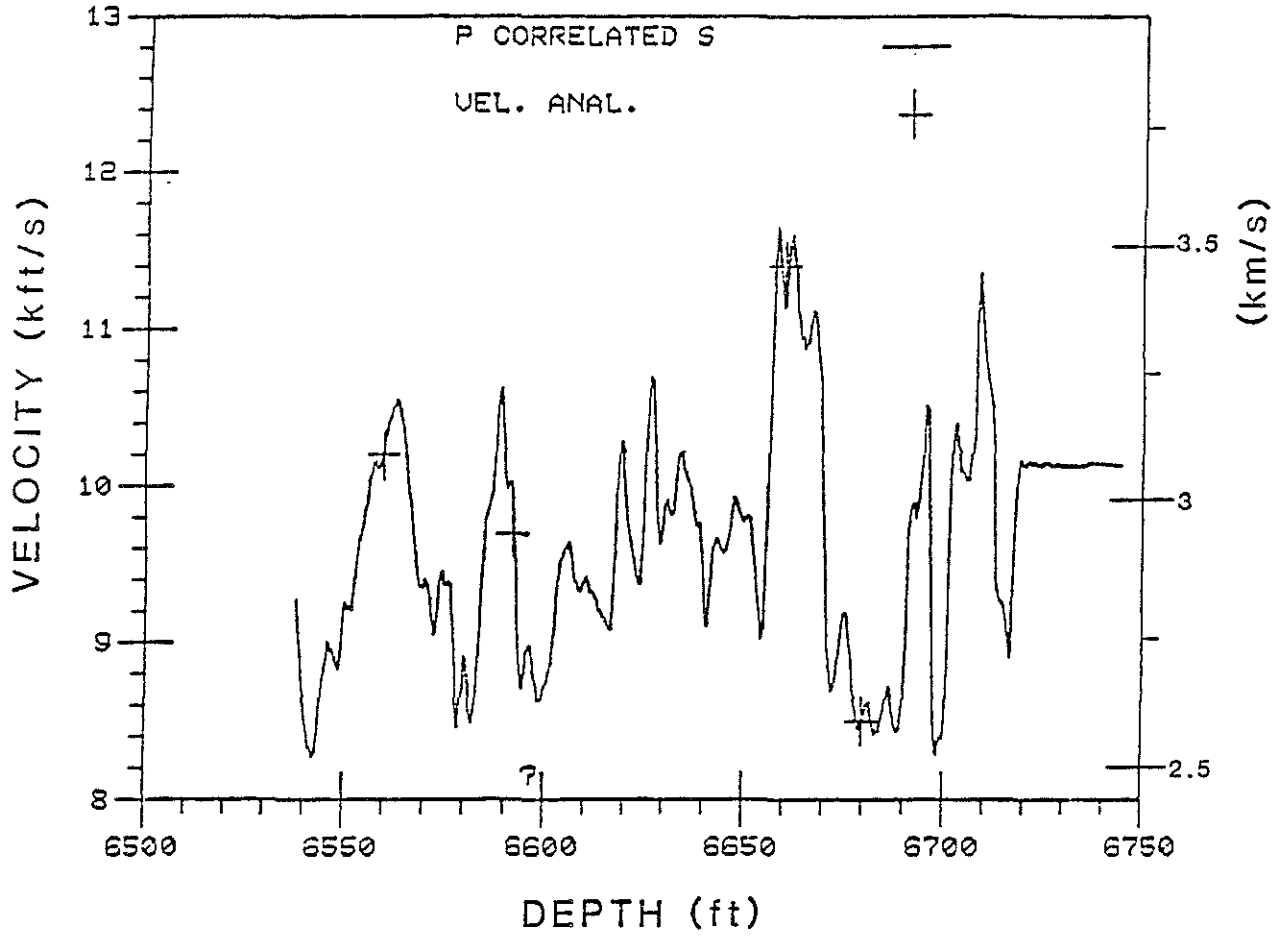

Figure 12a. Well log showing S velocities from four velocity analyses shown by crosses and P Correlated S velocities by the solid line.

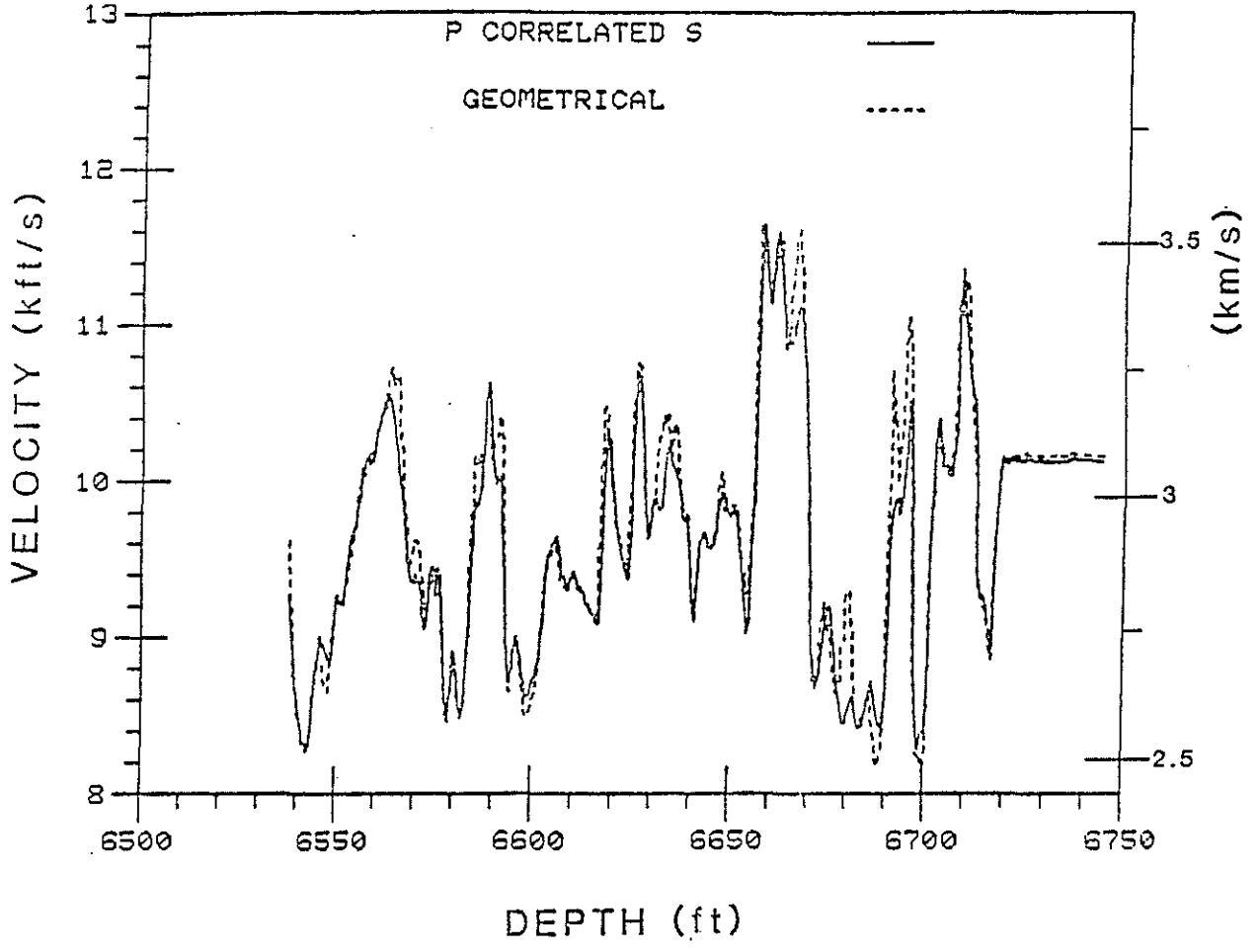

Figure 12b. Well log showing S velocities found by geometrical correlation (in dashed line) and by P Correlated S (solid line)

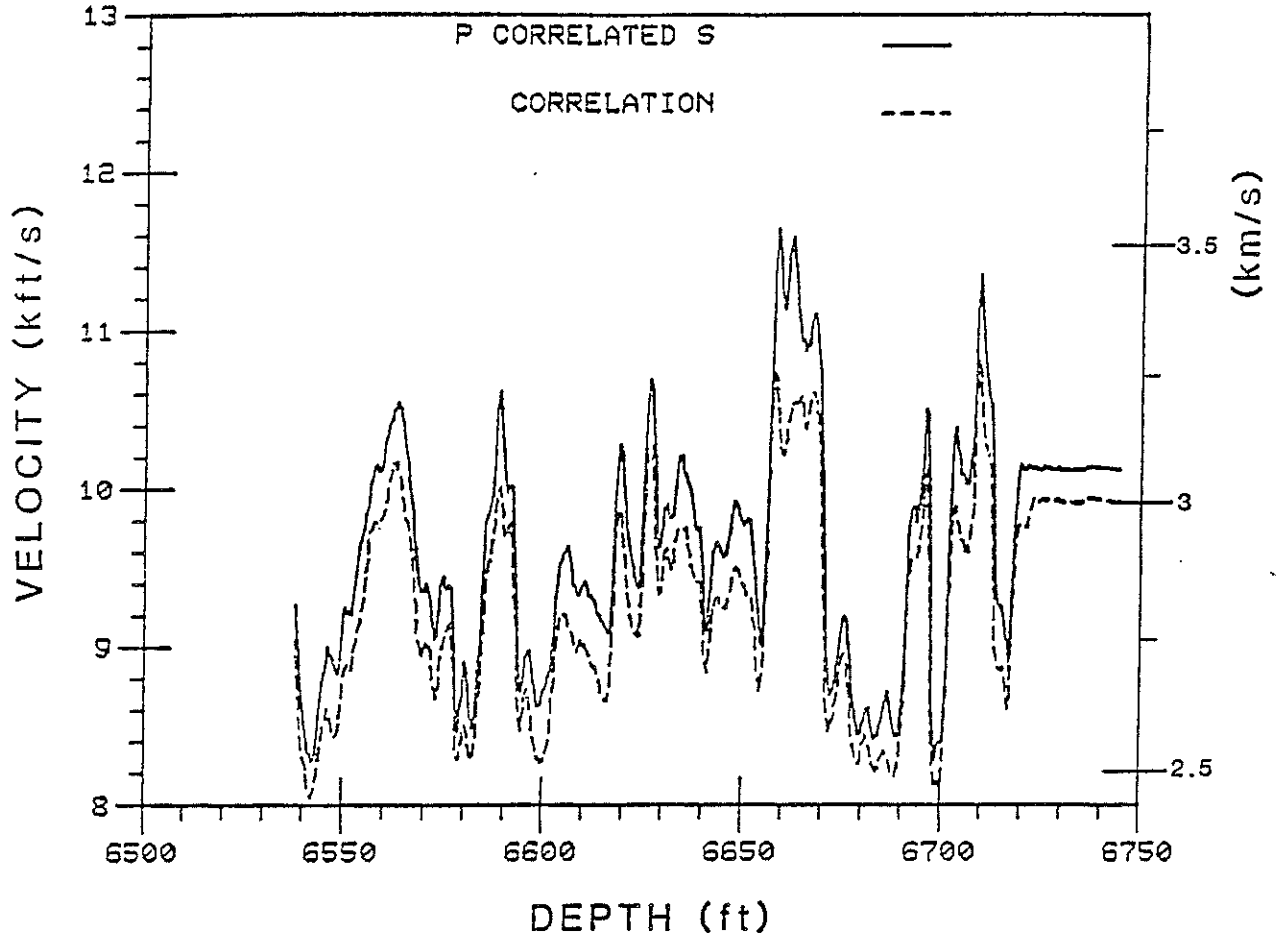

Figure 12c. Well log showing S velocities found by correlation (dashed line) and by P Correlated S (solid line).

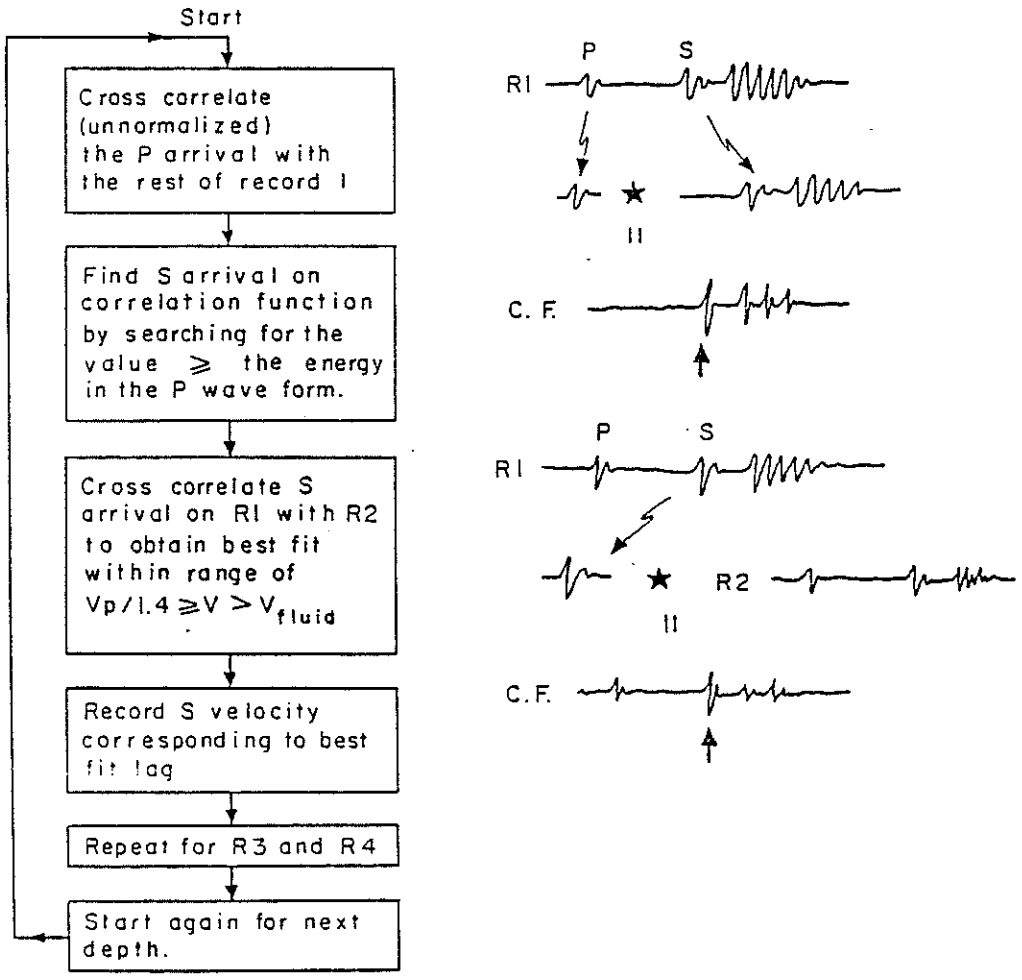

Figure 13. Computer flow diagram showing P Correlated S method of obtaining S velocities.

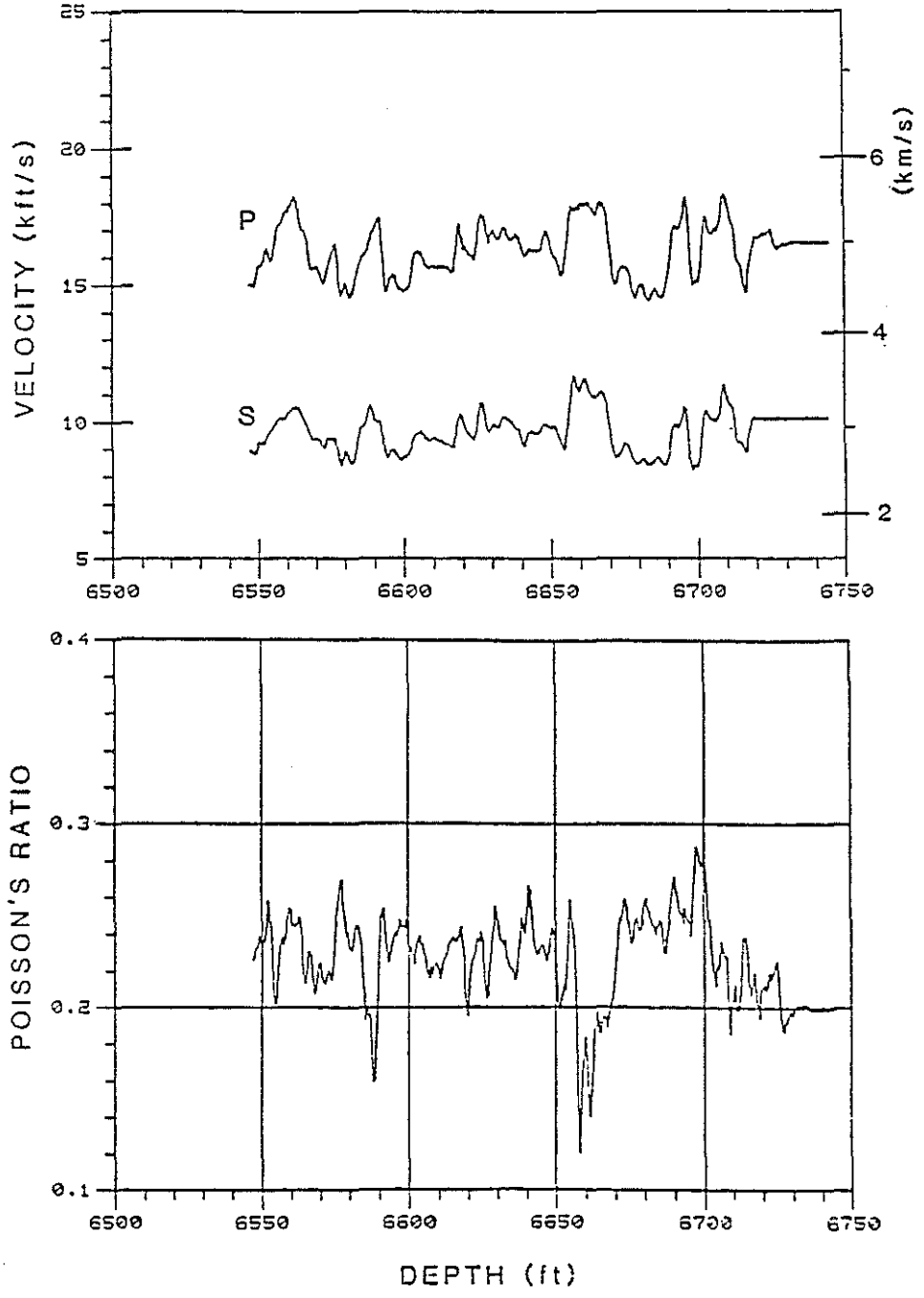

Figure 14. P and S wave velocities as obtained by compensated P wave method and P Correlated S method over a shale/sandstone sequence (top) and corresponding Poisson ratio profile (bottom).

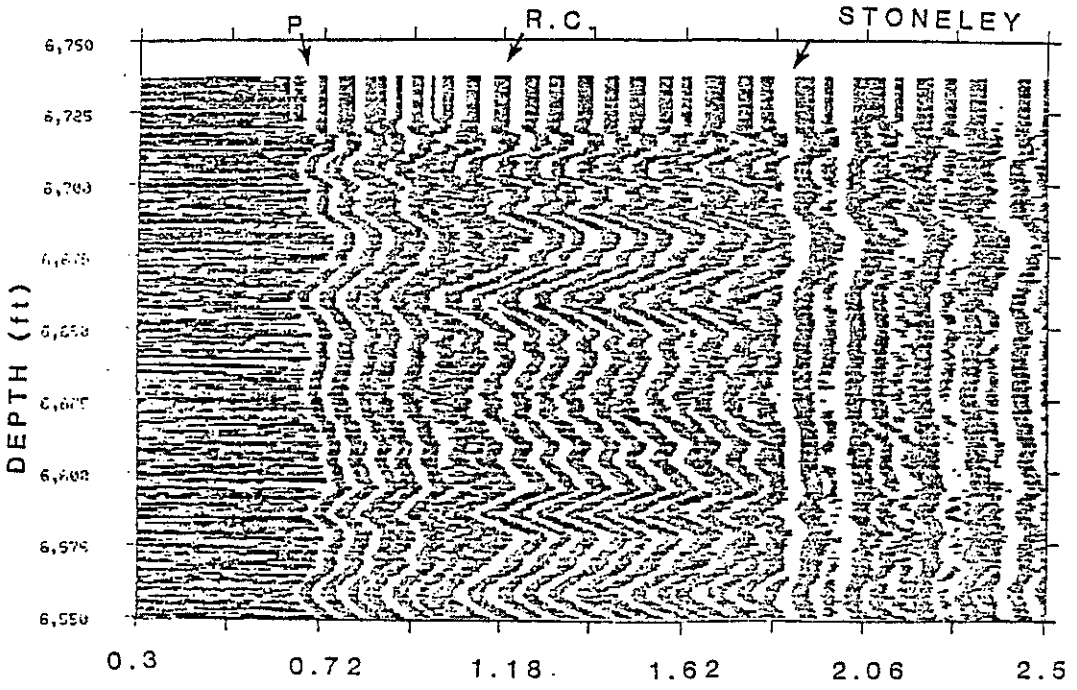

Figure 15. Sign bit plot of data from Well 1. Shown are the 10 foot waveforms from the top receiver. Positive amplitudes are dark, negative amplitudes are white.

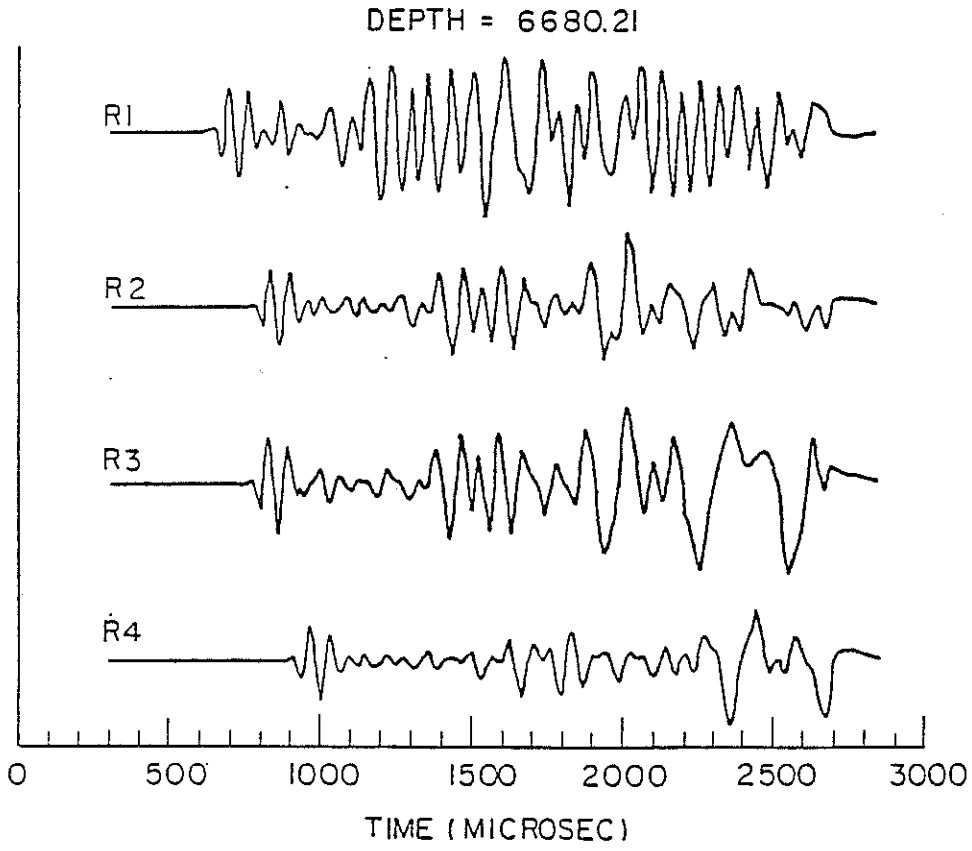

Figure 16. Plot of four waveforms from Well 1 at a depth of 6680.

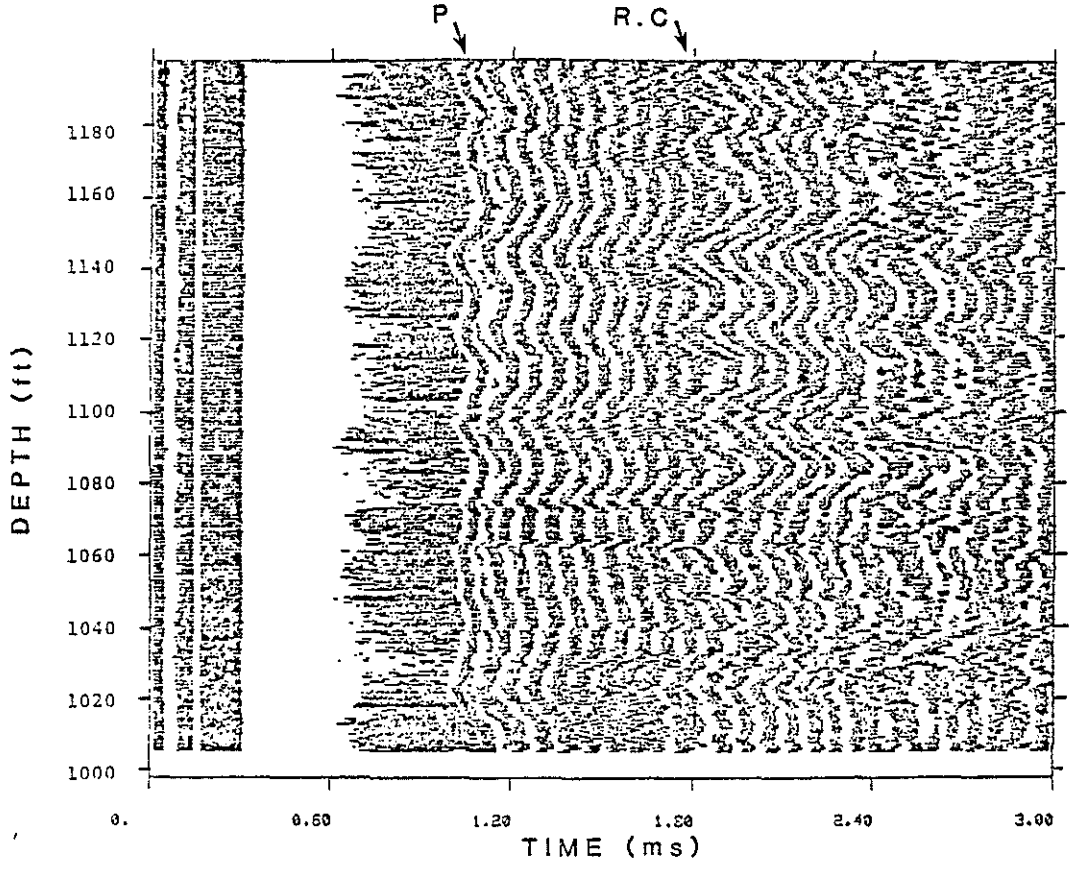

Figure 17. Sign bit plot of data from Well 2. Shown are the 10 foot waveforms from the top receiver. Positive amplitudes are dark, negative amplitudes are white.

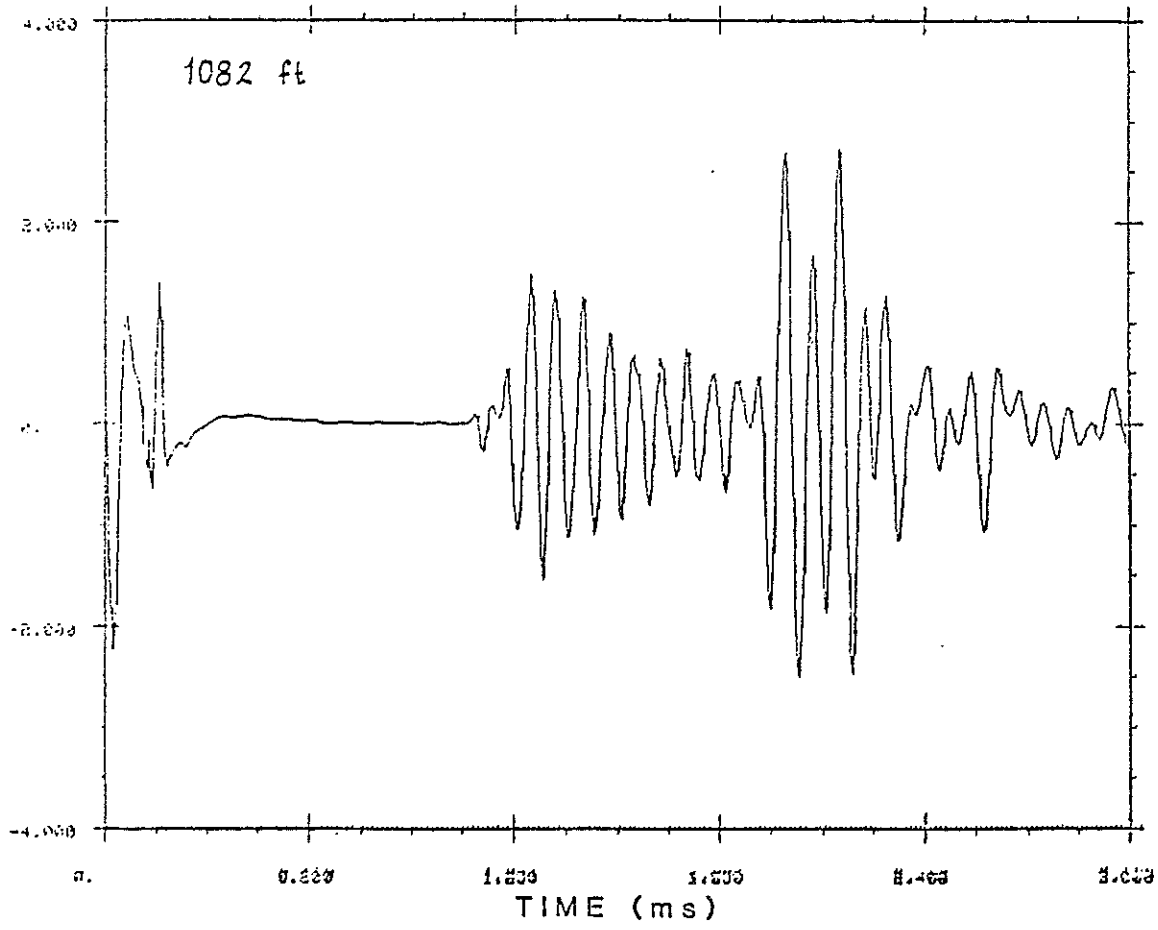

Figure 18a. 10 foot waveform from Well 2 at a depth of 1082 feet.

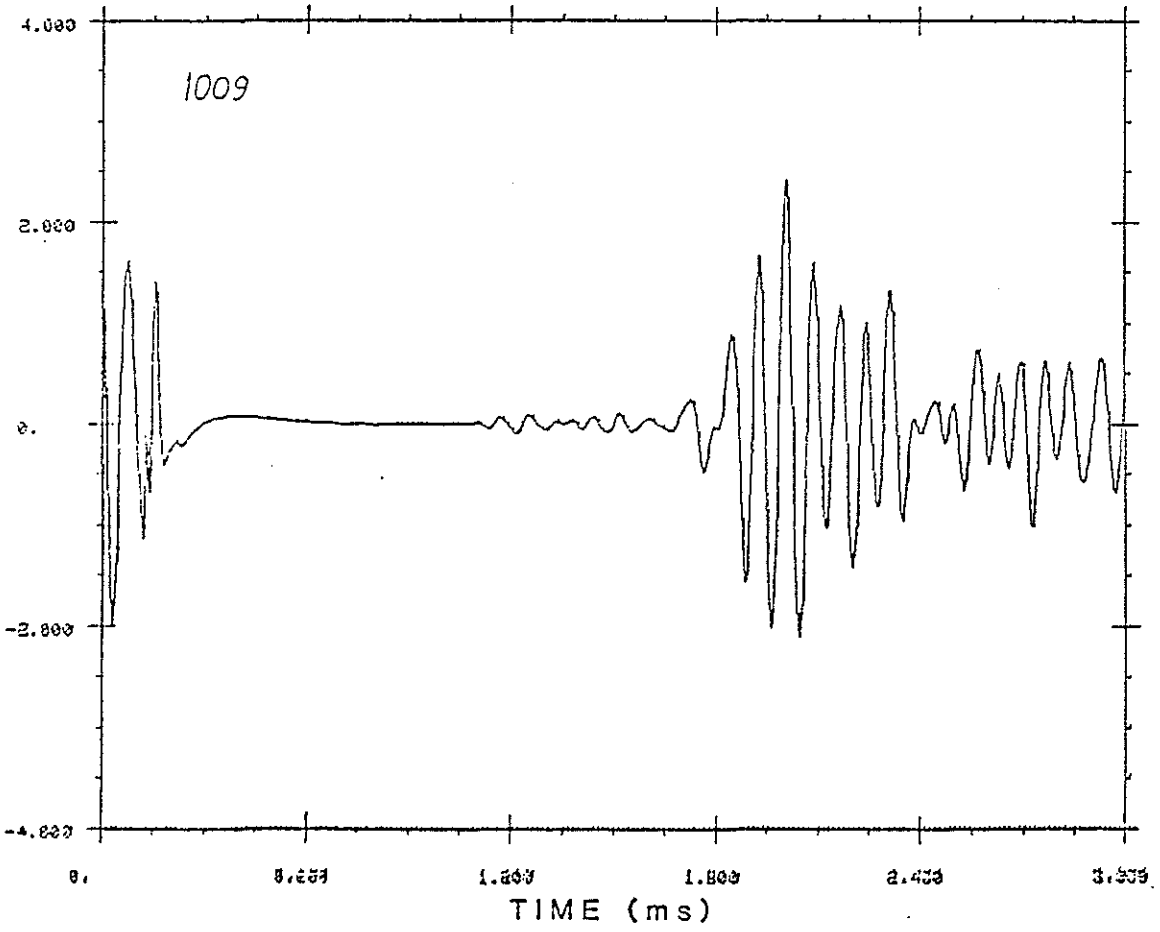

Figure 18b. 10 foot waveform from Well 2 at a depth of 1009 feet.

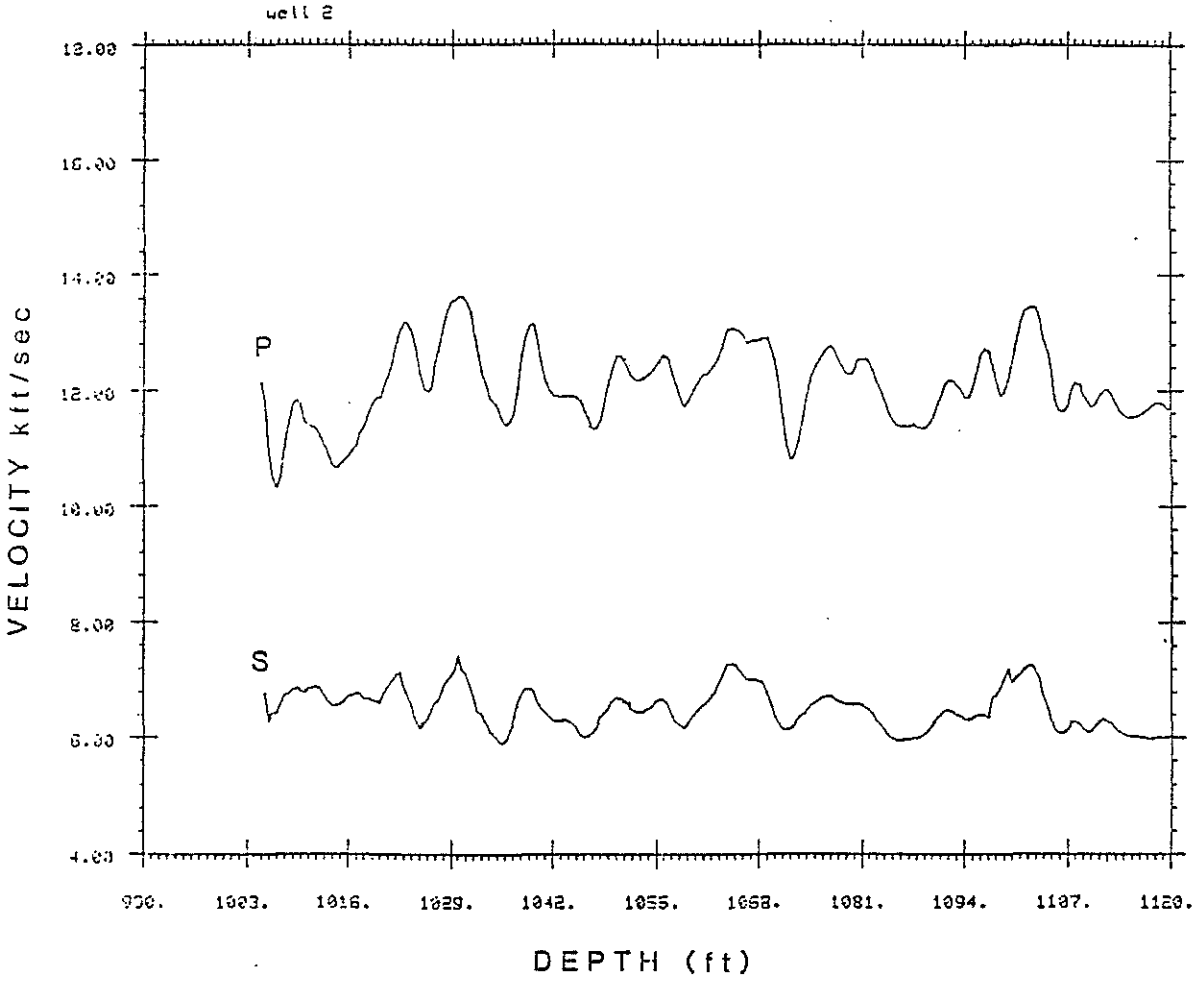

Figure 19a. Common source P and S velocity profile for Well 2.

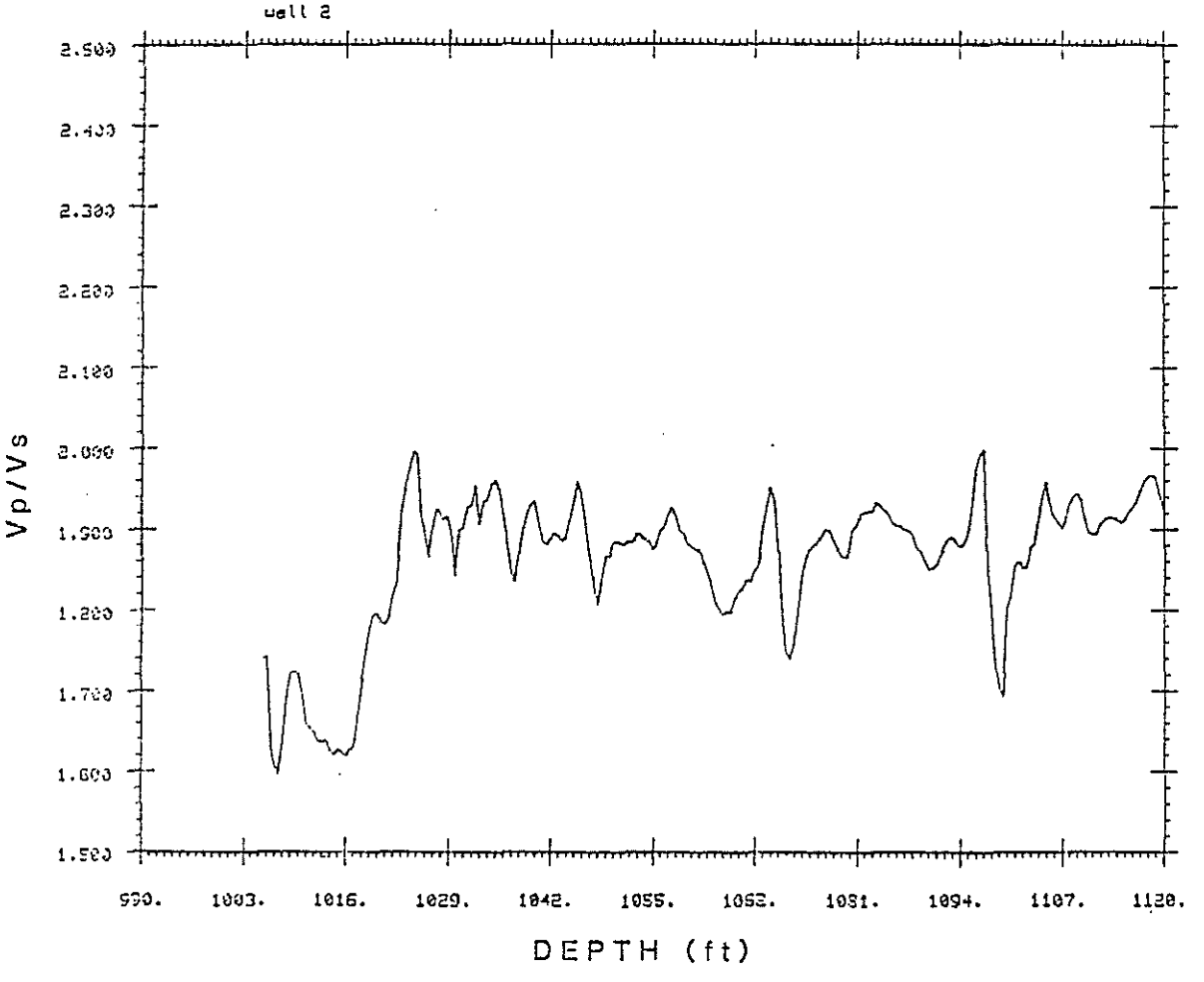

Figure 19b. α/β ratio profile derived from Figure 6a for Well 2.

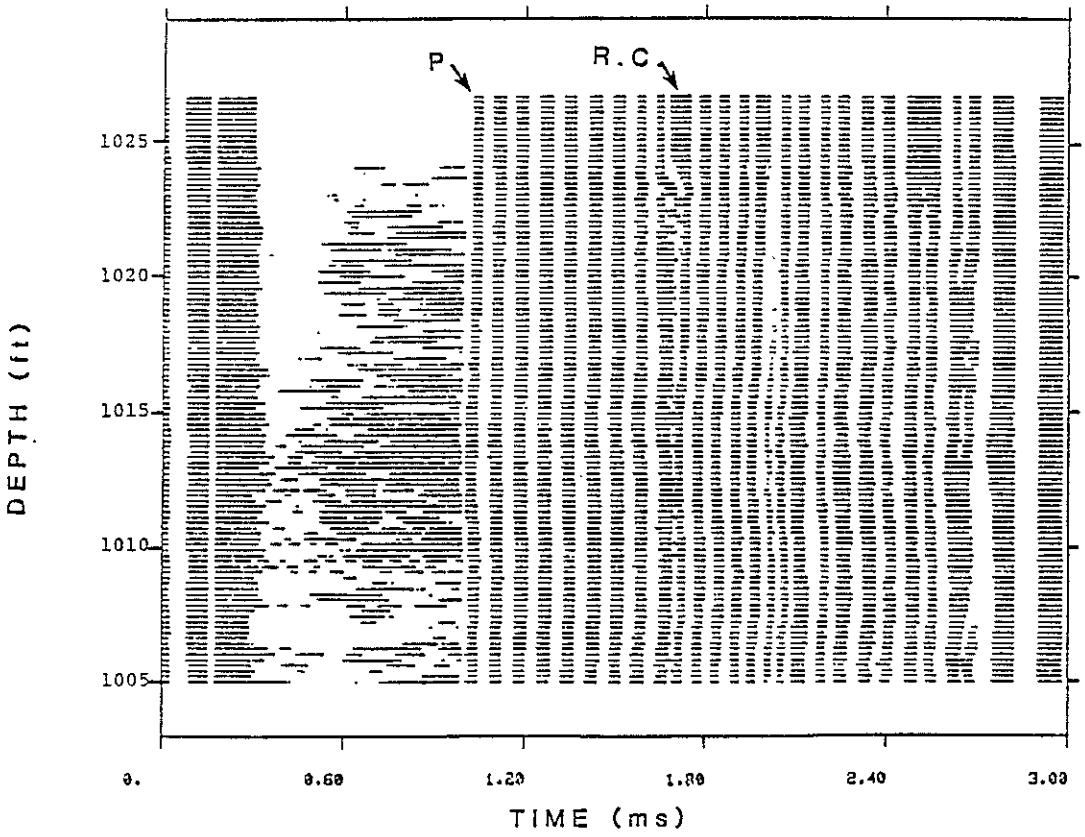

Figure 20. Sign bit plot of data from Well 3. Shown are the 10 foot waveforms. Positive amplitudes are plotted dark, negative amplitudes are plotted white.

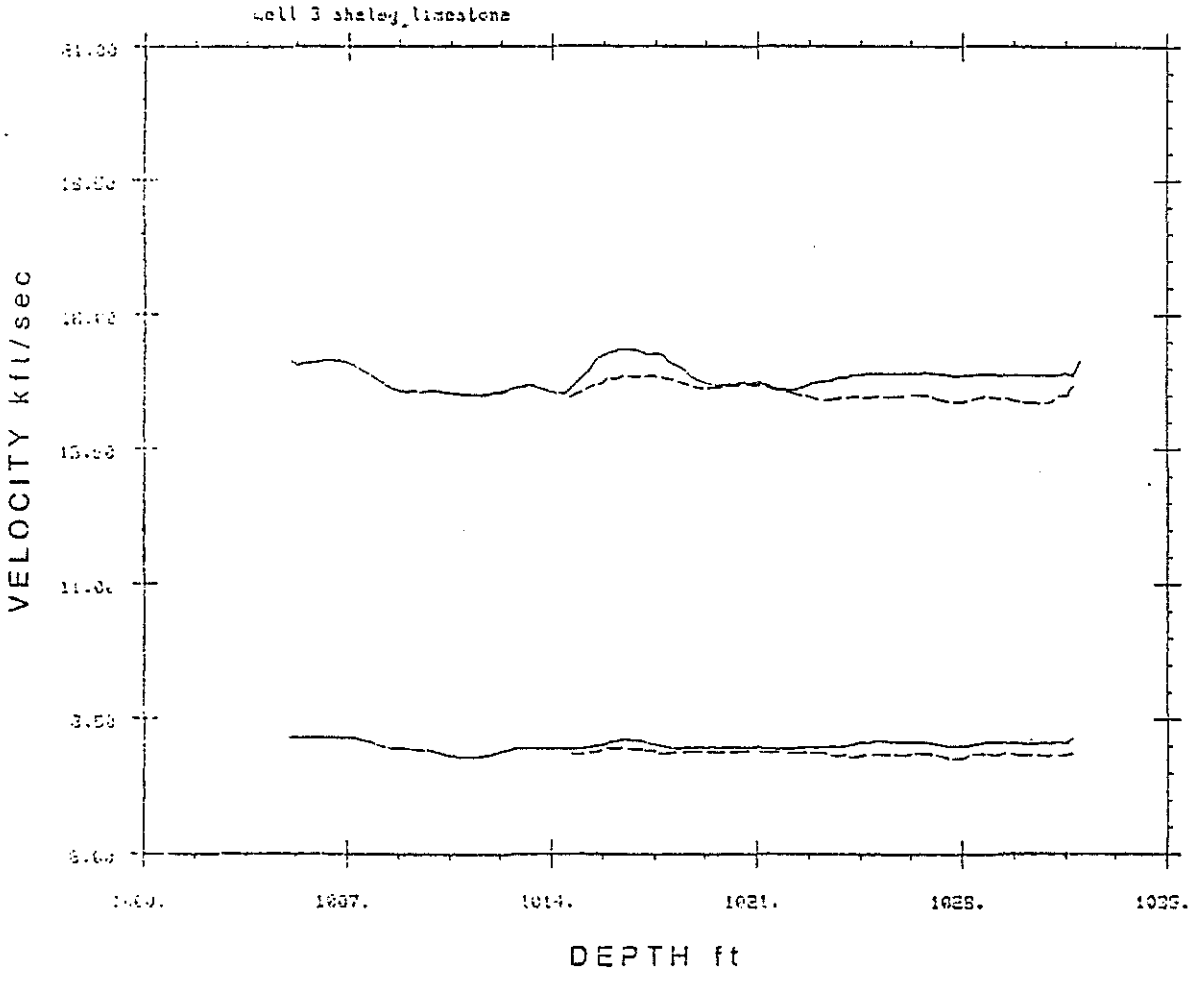

Figure 21a. P and S velocity profile for Well 3. Solid lines show common source velocities. Dashed lines show borehole compensated estimates.

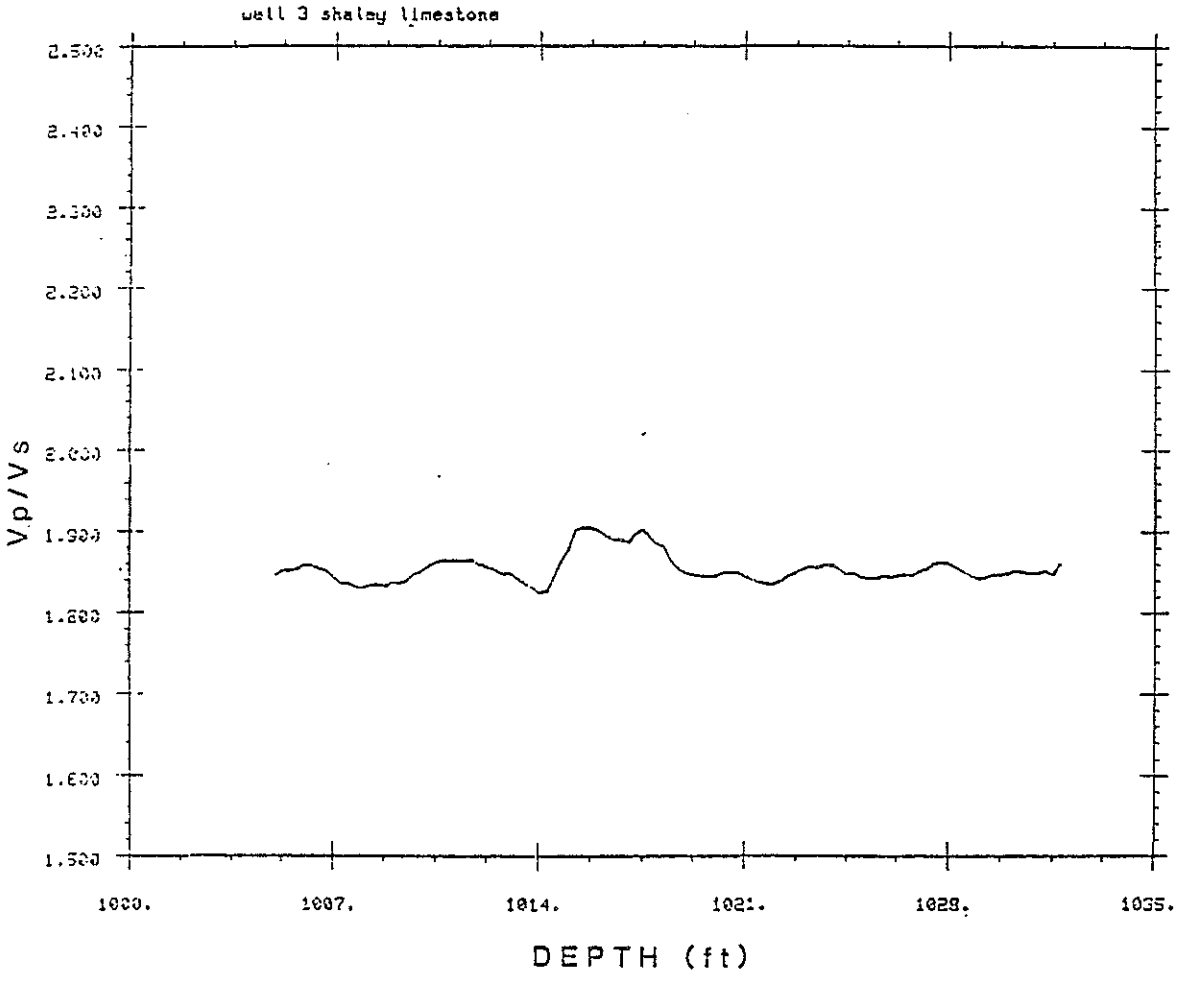

Figure 21b. α/β ratio profile for Well 3 using the common source velocities in Figure 21a.